

REPORT DOCUMENTATION PAGE			Form Approved OMB NO. 0704-0188		
<p>The public reporting burden for this collection of information is estimated to average 1 hour per response, including the time for reviewing instructions, searching existing data sources, gathering and maintaining the data needed, and completing and reviewing the collection of information. Send comments regarding this burden estimate or any other aspect of this collection of information, including suggestions for reducing this burden, to Washington Headquarters Services, Directorate for Information Operations and Reports, 1215 Jefferson Davis Highway, Suite 1204, Arlington VA, 22202-4302. Respondents should be aware that notwithstanding any other provision of law, no person shall be subject to any penalty for failing to comply with a collection of information if it does not display a currently valid OMB control number.</p> <p>PLEASE DO NOT RETURN YOUR FORM TO THE ABOVE ADDRESS.</p>					
1. REPORT DATE (DD-MM-YYYY) 18-06-2015		2. REPORT TYPE MS Thesis		3. DATES COVERED (From - To) -	
4. TITLE AND SUBTITLE Micro-Photoluminescence (micro-PL) Study of Core-Shell GaAs/GaAsSb Nanowires grown by Self-Assisted Molecular Beam Epitaxy			5a. CONTRACT NUMBER W911NF-11-1-0223		
			5b. GRANT NUMBER		
			5c. PROGRAM ELEMENT NUMBER 206022		
6. AUTHORS Md Shifat Us Sami			5d. PROJECT NUMBER		
			5e. TASK NUMBER		
			5f. WORK UNIT NUMBER		
7. PERFORMING ORGANIZATION NAMES AND ADDRESSES North Carolina A&T State University 1601 East Market Street Greensboro, NC 27411 -0001			8. PERFORMING ORGANIZATION REPORT NUMBER		
9. SPONSORING/MONITORING AGENCY NAME(S) AND ADDRESS (ES) U.S. Army Research Office P.O. Box 12211 Research Triangle Park, NC 27709-2211			10. SPONSOR/MONITOR'S ACRONYM(S) ARO		
			11. SPONSOR/MONITOR'S REPORT NUMBER(S) 59052-EL-REP.8		
12. DISTRIBUTION AVAILABILITY STATEMENT Approved for public release; distribution is unlimited.					
13. SUPPLEMENTARY NOTES The views, opinions and/or findings contained in this report are those of the author(s) and should not be construed as an official Department of the Army position, policy or decision, unless so designated by other documentation.					
14. ABSTRACT III-V NWs stand out due to their exceptional high electron mobility. The ability to grow in both axial and core-shell configurations in conjunction with band gap tuning as in the 2D structure make the NWs very attractive for next generation photo-detector, field-effect transistor (FET) and light emitting diode (LED) applications. In this thesis, room temperature and low temperature (4K) micro-photoluminescence (micro-PL) spectra of GaAs/GaAsSb ensemble NWs of single core-shell and double-shell configurations grown by molecular beam epitaxy will be presented. Experimental setup variables, namely detector type, objective lens magnification and chopper frequency.					
15. SUBJECT TERMS GaAsSb, Core Shell Nanowires, Micro Photoluminescence, Telecommunication Wavelength					
16. SECURITY CLASSIFICATION OF:			17. LIMITATION OF ABSTRACT	15. NUMBER OF PAGES	19a. NAME OF RESPONSIBLE PERSON
a. REPORT UU	b. ABSTRACT UU	c. THIS PAGE UU			Shanthi Iyer
					19b. TELEPHONE NUMBER 336-285-3710

Report Title

Micro-Photoluminescence (micro-PL) Study of Core-Shell GaAs/GaAsSb Nanowires grown by Self-Assisted Molecular Beam Epitaxy

ABSTRACT

III-V NWs stand out due to their exceptional high electron mobility. The ability to grow in both axial and core-shell configurations in conjunction with band gap tuning as in the 2D structure make the NWs very attractive for next generation photo-detector, field-effect transistor (FET) and light emitting diode (LED) applications. In this thesis, room temperature and low temperature (4K) micro-photoluminescence (micro-PL) spectra of GaAs/GaAsSb ensemble NWs of single core-shell and double-shell configurations grown by molecular beam epitaxy will be presented. Experimental setup variables, namely detector type, objective lens magnification and chopper frequency on micro-PL of these NWs were carefully examined to arrive at the optimized set up. Effect of Sb composition on the micro-PL spectra was studied. The dominant 4K PL peak varied from 1.35 eV to 0.99 eV with Sb concentration varying from 3 at.% to 26 at.%. The intensity dependence of micro-PL spectra at 4K enabled the development of band gap alignment in these structures. With increase in Sb composition type II hetero-alignment transitioned to type I alignment. NWs are observed to be curved with increasing Sb composition, which is attributed to the increased strain. PL system was suitably modified to acquire micro-PL spectra from a single NW. The system was made user friendly by adding a suitable attachment exterior to the optical system that facilitated motion of the laser in the nm range. micro-PL spectra of single NW replicated very well the respective NW ensemble, indicative of good compositional homogeneity of the NWs constituting the ensemble. Thus these NWs are very promising for near infrared optoelectronic device applications.

**Micro-Photoluminescence (μ -PL) Study of Core-Shell GaAs/GaAsSb Nanowires grown by
Self-Assisted Molecular Beam Epitaxy**

Md Shifat Us Sami

North Carolina A&T State University

A thesis submitted to the graduate faculty
in partial fulfillment of the requirements for the degree of

MASTER OF SCIENCE

Department: Nanoengineering

Major: Nanoengineering

Major Professor: Dr. Shanthi Iyer

Greensboro, North Carolina

2015

The Graduate School
North Carolina Agricultural and Technical State University

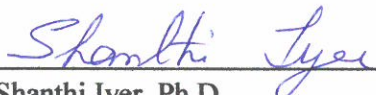
This is to certify that the Master's Thesis of

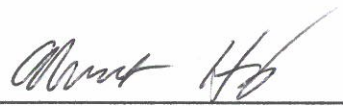
Md Shifat Us Sami

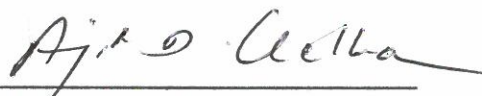
has met the thesis requirements of
North Carolina Agricultural and Technical State University

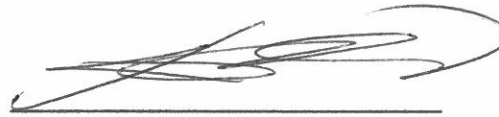
Greensboro, North Carolina
2015

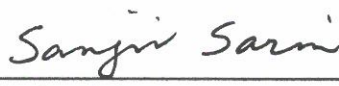
Approved by:


Shanthi Iyer, Ph.D.
Major Professor


Albert M. Hung, Ph.D.
Committee Member


Ajit Kelkar, Ph.D.
Department Chair


Sung-Jin Cho, Ph.D.
Committee Member


Sanjiv Sarin, Ph.D.
Dean, The Graduate School

Biographical Sketch

Mr. Md Shifat Us Sami, son of Mr. Md Abdus Satter Sarder and Mrs. Shirina Kohinoor, was born in 1988, Khulna, Bangladesh. He received his primary and secondary school education from Khulna Zilla School, Khulna, Bangladesh and his higher secondary school education from Notre Dame College, Dhaka, Bangladesh. He received his bachelor degree in Materials and Metallurgical Engineering from Bangladesh University of Engineering and Technology, Dhaka, Bangladesh. While in Bangladesh, apart from his studies he had lived a vibrant living style throughout his academic life. He was an executive committee member of the Student's Association for Materials and Metallurgical Engineering (SAMME). He worked for quite a few volunteer organizations namely Community Action, Badhon, Sheba, Aastha, and etc. and some of which he had co-founded. Mr. Md Shifat Us Sami came to the United States of America in August, 2013. Currently he is pursuing his master degree in Nanoengineering at the Joint School of Nanoscience and Nanoengineering, NC A&T State University, Greensboro, North Carolina. His research interest lies in semiconductor materials, ceramics, and nanotechnology. His vision is in pioneering inventions in the field of materials science and nanotechnology that will move the world towards a better future. Someday, he wishes to see himself as a prominent researcher in the field of materials science and engineering, and possibly as a research faculty member. He believes that fate can take a man anywhere and regardless of where he goes, he is committed to serve his best for mankind and be a better human every following day in his life.

To my parents.

Acknowledgments

Above all, I am grateful to The Almighty God for every breath I take. Then I am grateful to my family, for whom I am who I am today. I take pleasure to especially acknowledge a couple of people. First of all I am grateful to my advisor Prof. Shanthi Iyer, for her continuous support and representing herself as the role model for hard work. I am grateful to my research colleagues- Dr. Jia Li, Sai Krishna Ojha, Pavan Kumar Kasanaboina, Estiak Ahmad, Manish Sharma, Ngoc Nguyen, Briana McCall, Robert Alston and Prithviraj Deshmukh for their support and friendly attitude at all times. It has been my honor to work with them all. I am thankful to all my teachers, classmates, technical staff and everyone else at the JSNN who helped me towards achieving my goal. I am thankful to Ms. Karen Courtney for her motherly care to all the students at the Nanoengineering department. I am thankful to Ms. Diana Mejia for being such a sweet lady to us. I would never have come this far without the direct, or indirect help from any of these kindhearted people. I thank my landlord Mr. Larry Wallace and Mrs. Wendy Wallace, for providing me with the best living experience. I cannot ever repay Qassim Hassan for being my best friend at all times, and for his unconditional love, and I also thank Shuayl Alotaibi for sharing the warmth of friendship and love with us.

Funding of this work from ARO Grant No. W911NF-11-1-0223 (technical monitor-William Clark) is acknowledged.

Publications and Presentations

1. Kasanaboina, Pavan; Ojha, Sai Krishna; Sami, Shifat Us; Reynolds Jr, C; Liu, Yang; Iyer, Shanthi; “Bandgap Tuning of GaAs/GaAsSb Core-Shell Nanowires Grown by Molecular Beam Epitaxy" Nanotechnology, Article reference: NANO-106496 (Submitted)
2. Kasanaboina, Pavan; Ojha, Sai Krishna; Sami, Shifat Us; Reynolds Jr, C; Liu, Yang; Iyer, Shanthi; *Tailoring of GaAs/GaAsSb core-shell structured nanowires for IR photodetector applications* Proc. SPIE 9373, Quantum Dots and Nanostructures: Synthesis, Characterization, and Modeling XII, 937307 (February 27, 2015); doi:10.1117/12.2080572
3. Md Shifat Us Sami, JiaLi, Sai Krishna Ojha, Pavan Kumar Kasanaboina, Shanthi Iyer; “Micro-photoluminescence Study of Self-assisted MBE Grown Core and Core-Shell GaAs/GaAsSb Nanowires”, Poster submitted at the Nano Manufacturing 2014 – Conference at JSNN, Wednesday, September 24, 2014
4. Md Shifat Us Sami, JiaLi, Sai Krishna Ojha, Pavan Kumar Kasanaboina, Shanthi Iyer; “A Low Temperature Micro-photoluminescence Study of Self-assisted MBE Grown Core and Core-Shell Configured GaAsSb(N)/GaAs Nanowires for Nanoscale Photodetectors” , Poster submitted at the MRS/ASM/AVS Joint Symposium at NCSU, Friday, November 7, 2014

Table of Contents

List of Figures	xi
List of Tables	xvi
Abbreviations	xvii
Abstract	1
CHAPTER 1 Introduction	2
1.1 Objective.....	4
1.2 Approaches	4
CHAPTER 2 Literature Review	7
2.1 Background Theories.....	7
2.1.1 Bandgap in bulk materials	7
2.1.2 Bandgap in semiconductor materials.....	10
2.1.3 Emission from semiconductors	10
2.1.3.1 Excitons.....	10
2.1.3.2 Recombination mechanisms in semiconductor	11
2.1.4 Bandgap alignment and transitions in heterostructures	13
2.2 Group III-V Semiconductor NWs	13
2.2.1 Nanowire growth	14
2.2.2 Nanowire crystal structure.....	15
2.3 Photoluminescence of GaAs(Sb) Nanowires.....	15
2.3.1 Variation in low temperature (4K) μ -PL of ensemble of GaAs-GaAsSb heterostructured NWs for different Sb compositions	16
2.3.2 Intensity dependent μ -PL- Type I & type-II band alignment in heterostructures..	16
2.3.3 Temperature dependent μ -PL	17
2.3.4 Single nanowire μ -PL.....	17

CHAPTER 3 Methodology	18
3.1 Equipment and Tools	18
3.1.1 Laser	20
3.1.2 Optical microscope	20
3.1.3 Cryostation	21
3.1.4 Monochromator	21
3.1.5 Detector	21
3.1.6 Lock-in amplifier and chopper	21
3.2 Sample Preparation and Experimental Method	22
3.2.1 NW samples.....	22
3.2.2 μ -PL of ensemble of NWs	22
3.2.3 μ -PL of single NWs.....	22
3.3 Development of the Optical System Setup	25
CHAPTER 4 Results	26
Introduction.....	26
4.1 Variation in Low Temperature (4K) μ -PL of Ensemble of GaAs-GaAsSb Core-Shell Nanowires for Different Sb Compositions	27
4.2 Intensity Dependent μ -PL of Ensemble of GaAs/GaAsSb Nanowires	34
4.3 Temperature Dependent μ -PL of Ensemble of GaAs/GaAsSb Nanowires	38
4.4 Comparison of μ -PL Between Core-shell GaAs/GaAsSb and Core-shell With Passivation Layer GaAs/GaAsSb/GaAs Nanowires.....	40
4.5 μ -PL of GaAs-GaAsSb(N) Nanowires	41
4.6 μ -PL of Single NWs	42
4.7 Effect of Experimental Variables on μ -PL	44
4.7.1 Detector type and objective lens.....	44

4.7.1.1 Detection range.	44
4.7.1.2 Objective lens.	45
4.7.1.3 Detector noise level.	45
4.7.2 Chopper frequency	46
4.7.3 Integration time and number of scans	47
4.7.4 Focusing position.....	48
4.7.5 Effect of doing SEM before doing μ -PL	48
4.8 Special Phenomena and Challenges	49
4.8.1 NW melting phenomena.....	49
4.8.1.1 Burning of ensemble of NWs.....	49
4.8.1.2 Burning of single NWs.....	51
4.8.2 Laser peak.....	52
CHAPTER 5 Summary and Future Research	55
References	57

List of Figures

Figure 1. (a) Schematic showing the splitting of three energy states into allowed and forbidden bands of energies (b) Schematic showing the splitting of the 3s and 3p states of silicon into CB and VB. [20]	8
Figure 2. (a) Schematic showing the generation of positive (hole) and negative (electron) charges caused by electron jumping from VB to CB with the breaking of a bond (b) The E versus k diagram of the CB and VB of a semiconductor at (a) $T = 0$ K and (b) $T > 0$ K. [20]	8
Figure 3. Schematic showing bandgap of insulators, semiconductors and metals at $T = 4$ K. [21]	9
Figure 4. Energy band structures of (a) GaAs and (b) Si. [24]	10
Figure 5. Different types of recombination process- (a) Free to bound recombination (b) Donor-acceptor pair recombination (c) Trap-assisted recombination and (d) Auger recombination	12
Figure 6. Schematic band diagram for type-I and type-II heterostructure configurations.....	13
Figure 7. Self-assisted Vapour-Liquid-Solid Growth of GaAs Nanowires. (a) A thin film of SiO_x is prepared on the substrate. (b) The supplied arsenic initially desorbs, the diffusing Ga atoms form liquid droplets, which are immobilized by either pre-existing or Ga-etched pinholes in the SiO_x . (c) Once the droplets have formed, supersaturation of the Ga droplet with As leads to the crystallization of GaAs at the liquid-solid interface. [32].....	15
Figure 8. Schematic showing the μ -PL set up.	18
Figure 9. μ -PL setup in the Optics Lab.	19
Figure 10. Laser spot on the sample.	20

Figure 11. Optical micrographs of NWs deposited on substrate after sonication. (a) very few nanowires over SiO ₂ substrate due to underdoing of sonication, (b) large number of broken NWs and pile ups due to overdoing of sonication, deposited on p-type Si substrate, and (c) single NW deposited on TEM Cu mesh.	23
Figure 12. NW precipitate on (a) SiO ₂ substrate and (b) Cu grid after sonication. (c) p-type growth substrate after sonication (NWs are not observed).	24
Figure 13. (a) Sample placed inside the optical cryostation chamber. (b) Confocal microscope with the external mechanical nano-positioner.	25
Figure 14. Normalized low temperature (4K) μ -PL of ensemble of GaAs-GaAsSb core-shell nanowires for different Sb compositions.	27
Figure 15. Multi-peak fit for μ -PL of GaAs-GaAsSb core-shell NW with (a) Sb-1 at.%, (b) Sb-3 at.% (c) Sb-5 at.% (d) Sb-15 at.%, and (e) Sb-26.5 at.% compositions.	28
Figure 16. Gaussian fit of (a) Peak 1, (b) Peak 2, (c) Peak 3, (d) Peak 4, (e) Peak 5, (f) Peak 6, (g) Peak 7, and (h) Peak 8 for μ -PL of GaAs-GaAsSb core-shell NWs with different Sb compositions. Insets show the normalized form of the fitted peaks.	29
Figure 17. Shift in μ -PL peaks in core-shell GaAs-GaAsSb NWs with increasing Sb at.% composition.	31
Figure 18. Shift in PL peaks in core-shell GaAs-GaAsSb NWs with increasing Sb at.% composition.	32
Figure 19. (a) Core GaAs nanowires and (b) core-shell GaAs/GaAsSb nanowires. The insets show the respective side views of the NWs.	33
Figure 20. SEM images of single GaAs/GaAsSb core-shell nanowires for different Sb at.%.	33

Figure 21. Low temperature (4K) intensity dependent μ -PL of GaAs-GaAsSb core-shell NW with Sb-5 at.% composition.....	34
Figure 22. Multi-peak fit of low temperature (4K) intensity dependent μ -PL of GaAs-GaAsSb core-shell NW for different laser power intensities- (a) 63P, (b) 32P, (c) 16P, (d) 9P, and (e) 3P.	35
Figure 23. Change in peak position with multi-peak fit of low temperature (4K) intensity dependent μ -PL of GaAs-GaAsSb core-shell NW for different laser power intensities. The energy in horizontal axes are in log(2) scale.	36
Figure 24. Low temperature (4K) intensity dependent μ -PL of GaAs-GaAsSb core-shell NW with Sb-12 at.% composition.....	37
Figure 25. Low temperature (4K) intensity dependent μ -PL of GaAs-GaAsSb core-shell NW with Sb-3 at.% composition.....	37
Figure 26. Intensity dependent μ -PL of GaAs NW with GaAsSb insert of Sb-5 at.% composition (2014 data). Inset shows change in bandgap energy of the first peak around 1.35 eV with temperature and Varshni fit, superimposed with previous data [38].....	38
Figure 27. Intensity dependent μ -PL of GaAs-GaAsSb core-shell NW with Sb-3 at.% composition and GaAs-GaAsSb-GaAsSb double-shell NW with Sb-4.7 at.% composition in its GaAsSb shell. Inset shows the multifold increase in μ -PL signal between the two both at room temperature and 4K.	40
Figure 28. μ -PL of as-grown GaAs-GaAsSb(N) core-shell NW at room temperature and 4K. Inset shows the redshift and almost identical FWHM on normalized plot of the two curves.	41

Figure 29. Low temperature (4K) μ -PL of single and ensemble of GaAs-GaAsSb core-shell NWs with Sb-26.5 at.% composition. Inset shows the normalized curves.....	42
Figure 30. Room temperature and 4K μ -PL of single GaAs-GaAsSb(N) core-shell NW. Inset shows the result for ensemble of NWs for the same sample.	43
Figure 31. Low temperature (4K) μ -PL of ensemble of GaAs-GaAsSb-GaAs double-shell NWs with Sb-7~10 at.% composition. Inset shows the normalized curves.....	44
Figure 32. (a) Low temperature (4K) μ -PL of ensemble of GaAs-GaAsSb core-shell NWs, and (b) Room temperature μ -PL of ensemble of GaAs-GaAsSb(N) core-shell NWs.....	45
Figure 33. Low temperature (4K) μ -PL of two different NW ensembles that have similar peak intensity. Two different detector is used but the same lock in sensitivity of 0.5mV..	46
Figure 34. Room temperature μ -PL of ensemble of GaAs-GaAsSb(N) core-shell NWs for (a) different speed of chopper (b) different set of chopper.	47
Figure 35. Effect of integration time and average number of scans on μ -PL of NW.....	47
Figure 36. Shape of μ -PL for different focusing position.....	48
Figure 37. SEM images of ensemble of melted/burnt NWs (a) beginning of melting, (b) partially melted NWs; and (c) a single NW melting from the top.	49
Figure 38. A series of stacked μ -PL scans of ensemble of GaAs-GaAsSb core-shell NWs with Sb-3 at.% composition. Si detector and 50x non-IR lens was used.....	50
Figure 39. SEM images showing different modes of NWs burning after being exposed to high intensity laser for μ -PL (a) burning; (b) welding to the resting surface; and (c) spreading melt along edges.	51
Figure 40. A series of stacked μ -PL scans of a single GaAs-GaAsSb-GaAs double-shell NW at 4K. InGaAs detector and 50x-IR lens was used.	52

- Figure 41. 4K μ -PL of (a) Ensemble of GaAs-GaAsSb(N) core-shell NWs at two different positions. Inset shows the normalized plot of the two spectra. (b) Two different single GaAs-GaAsSb core-shell NWs. Inset shows the normalized plot of the two spectra. InGaAs detector and 50x-IR lens is used for both. 53
- Figure 42. Intensity dependent 4K μ -PL of ensemble of GaAs-GaAsSb core-shell NWs with dominant laser peaks. Inset shows the normalized plot of the spectra at lowest laser intensity..... 53
- Figure 43. Stacked scans of 4K μ -PL of a single GaAs-GaAsSb core-shell Sb-3.6 at.% composition NW with predominant laser peaks. 54
- Figure 44. Temperature dependent μ -PL of ensemble of GaAs-GaAsSb core-shell Sb-26.5 at.% NWs with predominant laser peaks. 54

List of Tables

Table 1	Change in core-shell GaAs-GaAsSb peak with Sb at.% composition	30
Table 2	Fit parameters for temperature dependence of semiconductor band gaps.....	39

Abbreviations

at. %	Atomic percent
E_g	Band gap energy
CB	Conduction band
Cu	Copper
EDS/EDX	Energy Dispersive X-ray Spectroscopy
FWHM	Full width half maxima
GaAs	Gallium Arsenide
GaAsSb	Gallium Arsenide Antimonide
GaSb	Gallium Antimonide
IR	Infrared
LED	Light Emitting Diode
MBE	Molecular Beam Epitaxy
MOVPE	Metalorganic Vapor Phase Epitaxy
μ -PL	Micro-photoluminescence
NIR	Near infrared
NW	Nanowire
SEM	Scanning electron microscope
VB	Valence band
VLS	Vapor Liquid Solid
WZ	Wurtzite
ZB	Zinc Blende

Abstract

III-V NWs stand out due to their exceptional high electron mobility. The ability to grow in both axial and core-shell configurations in conjunction with band gap tuning as in the 2D structure make the NWs very attractive for next generation photo-detector, field-effect transistor (FET) and light emitting diode (LED) applications. In this thesis, room temperature and low temperature (4K) micro-photoluminescence (μ -PL) spectra of GaAs/GaAsSb ensemble NWs of single core-shell and double-shell configurations grown by molecular beam epitaxy will be presented. Experimental setup variables, namely detector type, objective lens magnification and chopper frequency on μ -PL of these NWs were carefully examined to arrive at the optimized set up. Effect of Sb composition on the μ -PL spectra was studied. The dominant 4K PL peak varied from 1.35 eV to 0.99 eV with Sb concentration varying from 3 at.% to 26 at.%. The intensity dependence of μ -PL spectra at 4K enabled the development of band gap alignment in these structures. With increase in Sb composition type II hetero-alignment transitioned to type I alignment. NWs are observed to be curved with increasing Sb composition, which is attributed to the increased strain. PL system was suitably modified to acquire μ -PL spectra from a single NW. The system was made user friendly by adding a suitable attachment exterior to the optical system that facilitated motion of the laser in the nm range. μ -PL spectra of single NW replicated very well the respective NW ensemble, indicative of good compositional homogeneity of the NWs constituting the ensemble. Thus these NWs are very promising for near infrared optoelectronic device applications.

CHAPTER 1

Introduction

Miniaturization in modern semiconductor device components has brought us to ask the question- how small one can go and already there is a search for a next generation of components that will replace the traditional CMOS technology which is believed to have already crossed its peak of miniaturization on the economies of scale. [1] An overwhelming interest has been put during recent years on the research of semiconductor nanowires (NW) because it can be assembled without the need for complex and costly fabrication facilities and it has come a long way in the past two decades. [2] This novel one dimensional structure of semiconductor NWs are revolutionizing the optoelectronic materials world with their extreme flexibility in bandgap engineering through a wide selection of materials design architecture. [3] [4] [5]. They can efficiently transport charge (electrons and holes) and because of that they could function as building blocks for nanoscale electronics. The confinement in two dimension leads to unique density of electronic states profile resulting in with significantly different optical properties in comparison to the bulk material. In particular, the III-V NWs stand out with their exceptionally high electron mobility and possibility of low lasing threshold. [6] [7]. The ability to grow in both radial and axial configured structure in numerous compositions along with a wide choice of substrates enable efficient alloy bandgap engineering which made them potential candidate for variety of next generation device applications such as next generation photodetectors [8] [9] [10] [11], field-effect transistors (FETs) [12] [13] [14], and light emitting diodes (LEDs) [15] [16]. Especially enormous interest has been put in telecommunications in recent years where these NWs are sought to meet the ongoing demand of improvement in near infra-red (NIR) detection capability of photodetectors.

In contrast to the top down approaches that use traditional lithographic techniques, NWs are grown in a bottom up approach via direct synthesis on a substrate which ensures rational use of materials. [17] Molecular Beam Epitaxy (MBE) offers precise control over the non-equilibrium growths and is widely used for growing epitaxial thin films and NWs through Vapor-Liquid-Solid (VLS) mechanism, and also includes a wide variety of materials. It is possible to efficiently grow NWs with different radial and axial structural configurations like core-shell, axial inserts, or a combination of both. [3] [5] [18] [19]

GaAsSb NW is a group III-V material that has high electron mobility, and covers very important telecommunication wavelengths 1.3 μm and 1.55 μm in NIR region. It is a ternary alloy of GaAs and GaSb. There are several ternary and quaternary semiconductor materials that are active in the 1.3 μm and 1.55 μm optical window. Two material systems that are extensively studied for applications in the NIR region are InGaAs and GaAsSb. GaAsSb has several advantages over InGaAs. Due to the presence of a single group III element in GaAsSb (Ga instead of In and Ga), its electronic structure is less dependent on its alloy configuration. The electron lifetime in GaAsSb is larger and Auger recombination in GaAsSb is suppressed as compared to InGaAs. Also, Sb has surfactant nature so that GaAsSb can be used to improve the structural properties in GaAsSb. Thus, GaAsSb NWs are very promising for near infrared optoelectronic device applications. Since not much work has been done on optical properties of GaAsSb, it is important to research more rigorously on this material as the wavelength lies in the telecom wavelength range.

Photoluminescence is a spectroscopy technique providing information on bandgap, crystal structure and defects in semiconductor materials. In this thesis, a detailed study on micro-

photoluminescence (μ -PL) of self-assisted MBE grown GaAs-GaAsSb core-shell NWs is carried out at room and low (4K) temperatures, for different laser power intensities.

1.1 Objective. The objectives of this thesis are:

- ❖ *μ -PL setup for ensemble of NWs:* Working with a new setup to measure μ -PL at low temperature (4K) on ensemble of NWs instead of former practice of measuring normal PL on bulk NWs.
- ❖ *Transition to single NW μ -PL measurement setup:* Developing new methodology and successfully transforming from ensemble of NWs to single NW for μ -PL measurements.
- ❖ *User friendly setup:* Making the setup user friendly that will save enormous amount of time and effort, significantly increasing efficiency in μ -PL measurement.
- ❖ *Ascertaining effects of experimental variables:* Ascertaining the effects of various experimental setup variables to arrive at the optimum set up on general μ -PL.
- ❖ *Effect of Sb composition:* Ascertain the variation in optical properties of core-shell GaAs-GaAsSb NWs of different Sb composition.
- ❖ *Comparison of double shell over core-shell configuration:* To ascertain the effect of additional GaAs outer shell on the μ -PL spectral efficiency.

1.2 Approaches. Following approaches are taken to fulfill the objective of this thesis-

- *Sample for μ -PL:* The NWs used in this study are core-shell GaAs-GaAsSb grown by MBE. The Sb atomic percent (at.%) composition of the shell are varied for band gap engineering. Some NWs also have an added passivation shell layer of GaAs (double shell).

- *Sample preparation:* NW samples are properly cut into smaller pieces for carrying out μ -PL on ensemble of NWs. For single NWs, they are carefully ultrasonicated in alcohol solution and dried on Cu grid.
- *μ -PL:* μ -PL spectra are acquired on samples with different compositions .
 - The optical system has been developed to make it more user friendly. An external fixture has been set up for positioning the laser spot on the sample at the nano range.
 - Both the ensemble of NWs and single NW were examined. For single NWs μ -PL measurements, different type of substrates were used to avoid unwanted peaks in the spectra.
 - In selected sample PL was carried out in the entire temperature range of 4K-300K. Laser power intensity dependent μ -PL has been carried out to ascertain the band alignment of the heterostructure. μ -PL is carried out using different experimental variables to arrive at the optimum set up.
- *NW morphology and composition:* Scanning electron microscopy (SEM) was carried out on the samples to examine the morphology and electron dispersive spectrometer (EDS) attached to SEM was used to ascertain the NW composition.

The thesis consists of 5 Chapters. The following Chapter 2 begins with the background theory on band energy and review on semiconductor NWs, especially work related to the thesis. Chapter 3 discusses about the methodology adopted for getting μ -PL, the setup and variables, improvement in the setup, technical difficulties, and etc. Chapter 4 gives the μ -PL results as a function of Sb composition. It also gives the intensity dependence of the PL spectra and how the band alignment has been determined from the PL data. A comparison of the double shell to

single shell has been made. Consistency of the results between the μ -PL of ensemble of NWs and single NW are shown. Effects of various experimental set up variables on μ -PL are also carefully examined. The final Chapter 5 summarizes the outcome of the thesis and outlines future direction of research.

CHAPTER 2

Literature Review

The formation of this section begins with background theories and definitions of semiconductor bandgap energy followed by review on III-V semiconductor NWs, NW growth techniques, and optical properties. Then an overview of the research related to the μ -PL of GaAs-GaAs(Sb) core-shell NWs is presented.

2.1 Background Theories

2.1.1 Bandgap in bulk materials

When two atoms come in close proximity to each other, their wave functions overlap and electrons begin interacting. This interaction results in discrete quantized energy level splitting into different sets of discrete energy levels, which is consistent with the Pauli Exclusion Principle that no two electrons can occupy the same electronic state. Each set of discrete energy levels is called an allowed energy band and the gap in between two such sets is called forbidden energy band. A qualitative image of the splitting of these discrete energy levels into allowed and forbidden energy bands in an atom as it approaches another is shown in Fig. 1(a). For bulk materials, quantum states in the outer shell of atoms participate in the splitting and they are divided into two major bands, one of which is completely filled with electrons at the absolute zero temperature i.e. $T = 0$ K which is called the valence band (VB), while the other is completely devoid of electrons at $T = 0$ K which is called the conduction band (CB). The formation of these energy bands is governed by the electrical characteristics of the crystal. Figure 1(b) shows the band splitting of Si, the atoms of which are covalently bonded. Here the outer 3s and 3p shell quantum states (eight in total) divide into CB with four vacant quantum states and VB with four states filled with electrons at $T=4$ K.

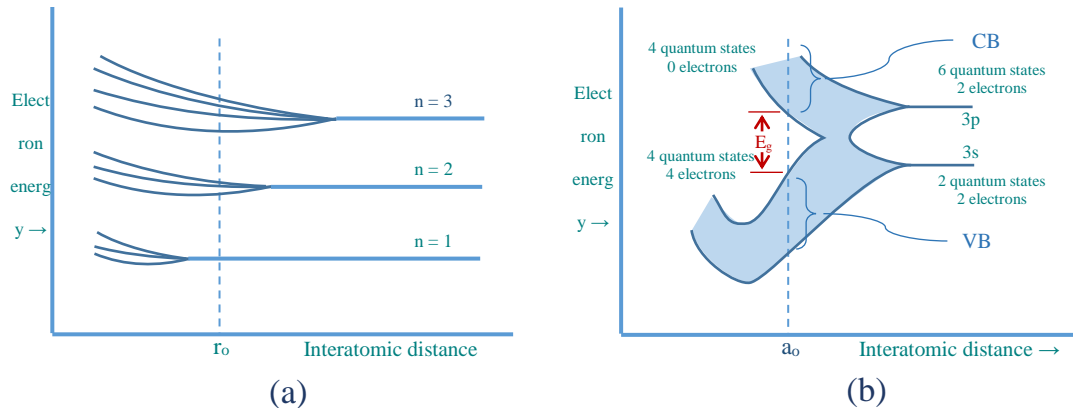


Figure 1. (a) Schematic showing the splitting of three energy states into allowed and forbidden bands of energies (b) Schematic showing the splitting of the 3s and 3p states of silicon into CB and VB. [20]

As the temperature goes up or, if the material is illuminated with light of enough energy, few VB electrons may gain sufficient thermal energy to break through the bond and jump up from the VB to the CB energy states. This leaves a positive hole in the VB and creates a negative charge in the CB which is shown in the schematics of Fig. 2(a). The energy of electrons are best described by the particle momentum, as $E = p^2 / 2m^*$ where $p = \hbar k$, k is the wave number, \hbar is the Plank's constant, and m^* is the effective mass of the conduction band. E-k band diagram is shown in Fig. 2(b).

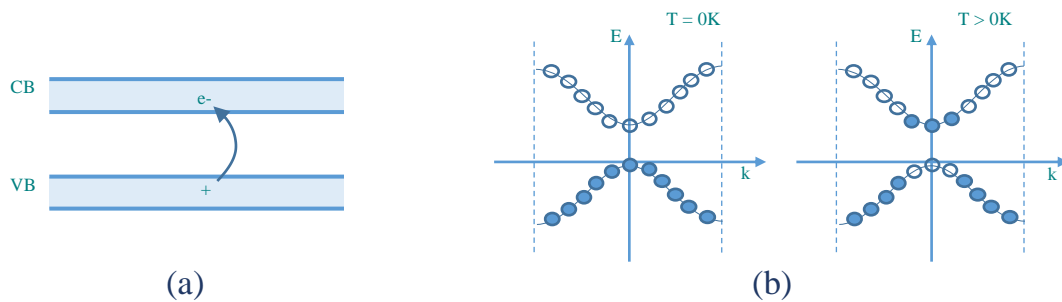


Figure 2. (a) Schematic showing the generation of positive (hole) and negative (electron) charges caused by electron jumping from VB to CB with the breaking of a bond. (b) The E versus k diagram of the CB and VB of a semiconductor at (a) $T = 0$ K and (b) $T > 0$ K. [20]

Bandgap is a distinct characteristic which is fundamentally different in metals, semiconductors and insulators. For metals, the CB and VB are actually partially overlapped so there is always some electron available at the CB. In contrast, for insulators the bandgap (usually > 10 eV) is so large that it takes a lot of energy for an electron to jump up from VB to CB. The bandgap of semiconductors is interesting in the fact that they are not overlapping yet being so narrow (usually < 4 eV) that excitation of electrons from VB to CB is possible with reasonable thermal/optical energy, and some charges can be present at room temperature that makes them conductive like metals at high temperatures and behave like insulator at 0K. Figure 3 shows the bandgap of semiconductors, metals and insulators at 4K.

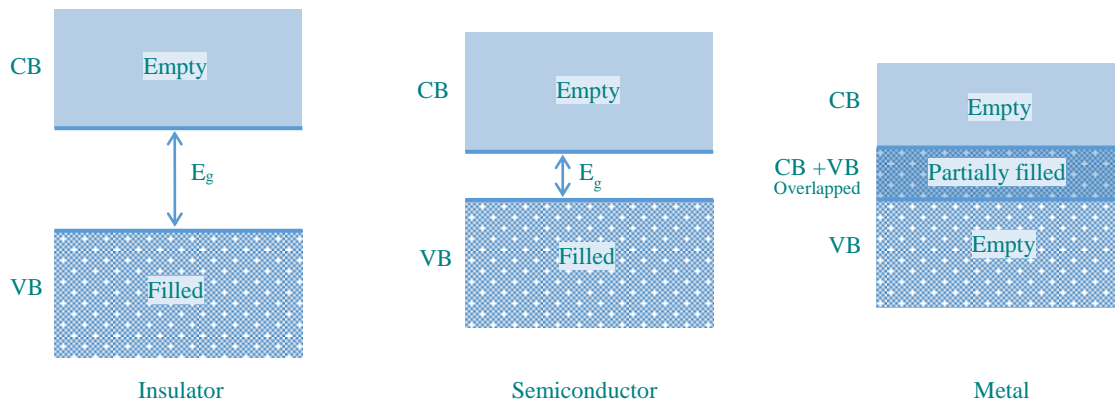


Figure 3. Schematic showing bandgap of insulators, semiconductors and metals at $T = 4K$. [21]

The energy level (if it exists) that has a 50% chance of being filled at any temperature is called the Fermi energy level of that material. [22] This definition of Fermi level especially holds for semiconductor materials. Also, for crystalline materials energy levels can be present in between the CB and VB when defects are present. It is also possible for the Fermi level to get pinned at a particular position because the surface/interface that can act as a source or sink of defects. [23]

2.1.2 Bandgap in semiconductor materials

Depending on the type of electron transition from VB to CB and vice versa, semiconductor bandgaps are classified as either direct bandgap, where an electron at the lowest energy point of CB has the same momentum as that of the highest energy point of VB on the E-k diagram (refer to Fig. 2(b)) as in GaAs, or indirect bandgap, where the lowest energy point of CB does not have the same momentum as that of the highest energy point of VB as in Si (Fig. 4).

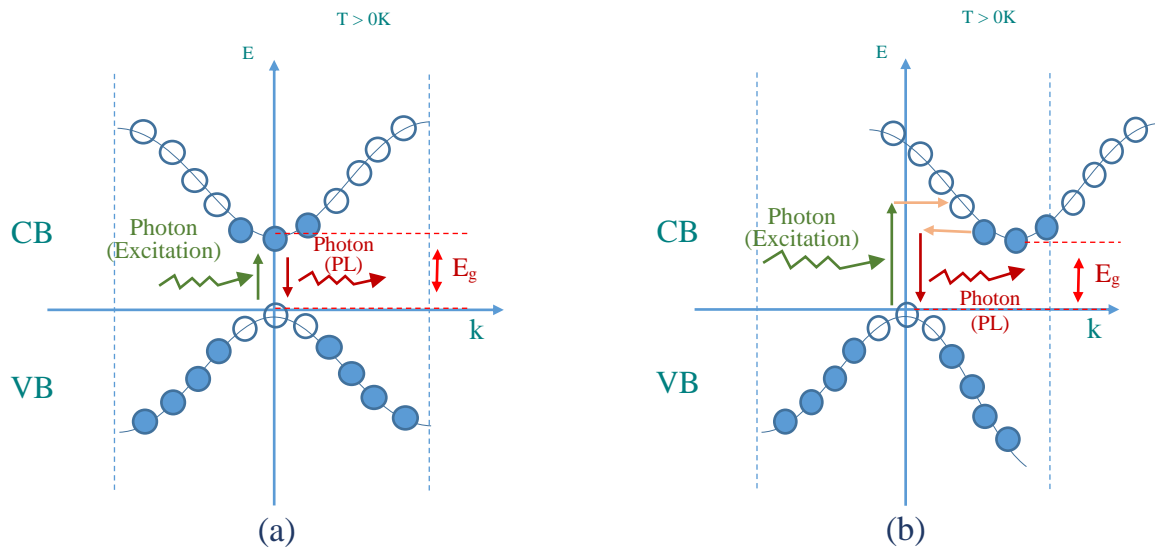


Figure 4. Energy band structures of (a) GaAs and (b) Si. [24]

2.1.3 Emission from semiconductors

While emissions from semiconductors at low temperatures are mainly attributed to the mechanism of creation of excitons for most of the materials, several other recombination mechanisms (i.e. decay of excitons) may also play role in emission. These two processes of emission are explained as follows.

2.1.3.1 Excitons

A free electron in the CB of a semiconductor and a free hole in the VB attract each other by electrostatic Coulomb force and they can be bound in a state of quasiparticle that is

electrically neutral because they have no net charge. [25] These quasiparticles are called excitons. Being bound to each other in space, these free electrons and holes are unable to move freely in solid and their potential energy is both lowered due to the amount of energy required in the formation of the free exciton that is called exciton binding energy.

Unlike recombination mechanism where a free hole at the top of the VB and a free electron at the bottom of the CB recombine to emit the same energy photon as that of the bandgap, excitons emit slightly lower energy photons because of the energy spared as exciton binding energy. For instance, the exciton binding energy in GaAs is 4.2 meV, which means that emission energy from a free exciton annihilation would be 4.2 meV lower than the bandgap energy. [26]

Emission energy from excitons can be further reduced when they become bound to an ionized or neutral impurity. This gives rise to sub-bandgap radiation that can provide valuable information about the type of impurity and in turn, about the material quality. For example, lines from excitons bound at ionized and neutral Zn in GaAs are reported to be found at 31.2 ± 0.4 , and 8.0 ± 0.3 meV below bandgap energy. [27]

2.1.3.2 Recombination mechanisms in semiconductor

Recombination mechanisms in a direct bandgap semiconductor can broadly be classified into two groups, radiative and non-radiative. Radiative recombination occurs when an electron from the CB recombines with a hole in the VB and emits the excess energy in the form of a photon. Radiative recombination can be spontaneous, absorption, or stimulated in type. The latter forms the basis for laser action in which the emitted photon has the same energy and momentum as the incident photon. [28]

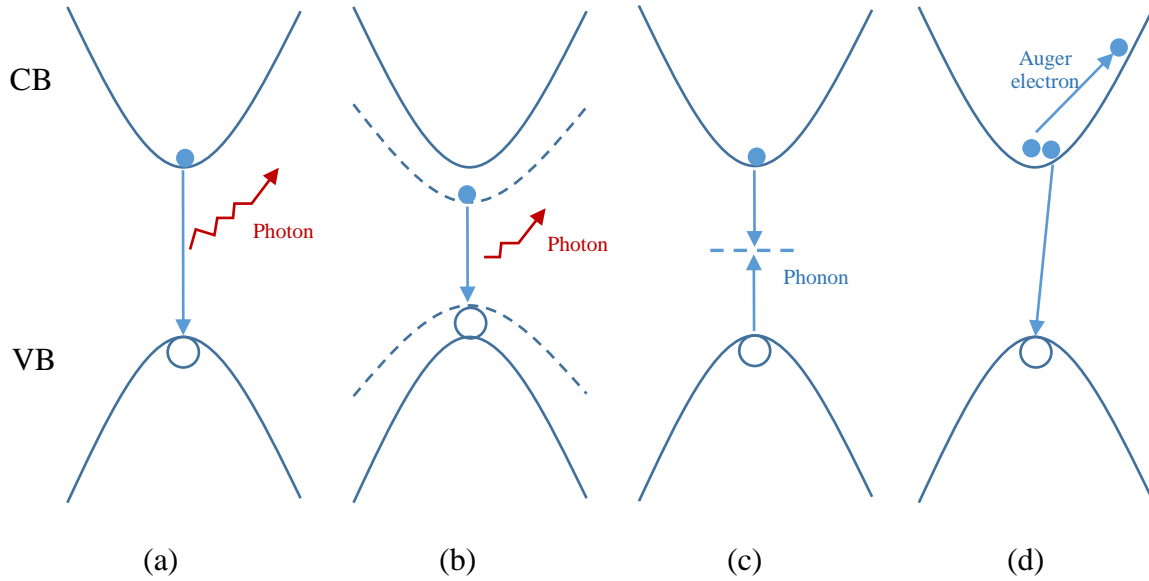


Figure 5. Different types of recombination process- (a) Free to bound recombination, (b) Donor-acceptor pair recombination, (c) Trap-assisted recombination, and (d) Auger recombination

In the radiative recombination where an electron from CB directly recombines with a hole in VB emits photon with same energy as that of the bandgap energy (Fig. 5 (a)). Free-to-bound recombination involve the radiative recombination of a free carrier with a carrier which is bound to an impurity. If the free carrier is a hole in VB, then it can be bound to an acceptor and if the free carrier is an electron in CB, then it can be bound to a donor. The donor-acceptor pair emission thereby occurs below the bandgap and depends upon the relative energy difference between the two impurity-bound pairs at the donor and acceptor level. (Fig. 5 (b)). Trap-assisted recombination is called Shockley-Read-Hall recombination, and is mostly non-radiative in nature (Fig. 5 (c)). The last type is the Auger recombination where an electron and a hole recombine in a band-to-band transition and give off the resulting energy to a third particle e.g. another electron or hole. It is different from typical band-to-band transition because of the involvement of the third particle leading to non-radiative recombination and found to be the major cause for ‘efficiency droop’ in LED. (Fig. 5(d)).

Excitons usually give rise to narrow emission lines. On the other hand the recombination mechanisms mentioned above in Figs. 5(b) and (c) give rise to broad emission lines and the emission in Fig. 5(d) gives rise to quenching of the emission. These remarks are very useful in identifying the recombining species. [29]

2.1.4 Bandgap alignment and transitions in heterostructures

When two different semiconductor materials with two different bandgaps are used to form a heterostructure, there can be two different types of transitions between them. When the transition is within the CB and VB of the same material that is called type-I transition and for electron transfer from the CB of one material to the VB of other is referred to as type-II transition. . Figure 6 shows the schematic of typical type-I and type-II transitions between zinc blende (ZB) GaAs and ZB GaAsSb heterostructures under strained condition.

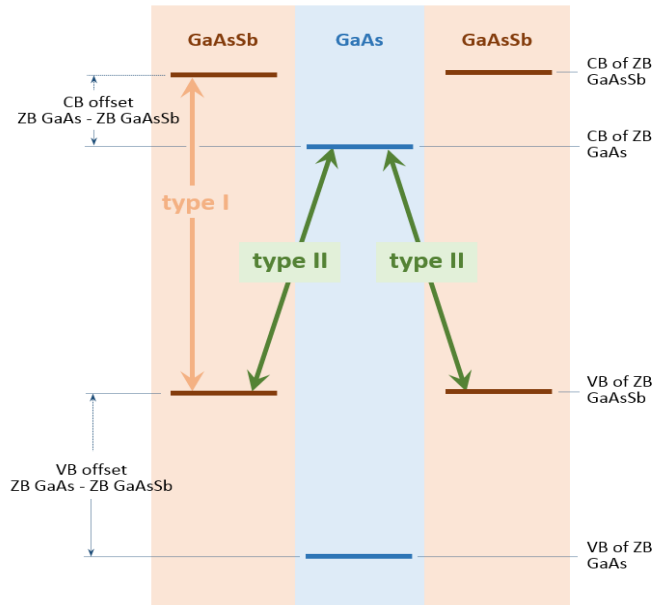


Figure 6. Schematic band diagram for type-I and type-II heterostructure configurations.

2.2 Group III-V Semiconductor NWs

An overview on the growth, characterization and optical properties of GaAs core and GaAs-GaAsSb core-shell heterostructure NWs are presented in this section.

2.2.1 Nanowire growth

Nanowires can be grown via various techniques. It can follow either the traditional top down approach using lithography, or the NWs can be directly grown on the substrate following bottom up approach which is the most popular practice. [30] So far various bottom up fabrication methods have been employed to grow group III-V NWs, most of which follow vapor-liquid-solid (VLS) mechanism. Among the most popular growth techniques that use the VLS mechanism are molecular beam epitaxy (MBE) [4] and metal organic chemical vapor deposition (MOCVD) [31]. The NWs related to this thesis are grown in molecular beam epitaxy (MBE) which is widely used, especially in research because of its highest achievable purity and most precise external controllability.

The VLS mechanism is especially suited for growth of thin layers and one-dimensional structures such as NWs. As the name suggests, the growth mechanism involve three distinct phases- a vapor phase through which the material is transported from source to substrate, a catalytic liquid phase which acts as a source of nucleation to grow NWs which is usually in droplet form, and the solid NWs that grow in the axial direction as the core. The catalytic liquid alloy phase reaches to super-saturation levels by quickly absorbing the vapor, and the material grows at the solid-liquid interface through formation of seed and subsequent precipitation of the supersaturated alloy. The growth is called self-assisted, when the liquid droplet itself is one element from the alloy crystallizing, or it is called catalyst assisted when another neutral element is used as the catalyst droplet (usually Au). A schematic of the self-assisted one dimensional growth of GaAs NWs is shown in Fig. 7. Here Ga droplet is used as the self-catalyst. The NWs can be radially grown as shell which involves some kinetics from thermodynamics. However, the details of the growth are outside the scope of this thesis and are not explained.

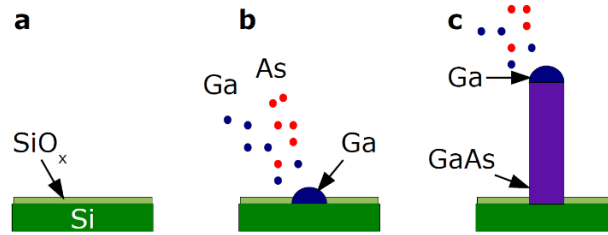


Figure 7. Self-assisted Vapour-Liquid-Solid Growth of GaAs Nanowires. (a) A thin film of SiO_x is prepared on the substrate. (b) The supplied arsenic initially desorbs, the diffusing Ga atoms form liquid droplets, which are immobilized by either pre-existing or Ga-etched pinholes in the SiO_x. (c) Once the droplets have formed, supersaturation of the Ga droplet with As leads to the crystallization of GaAs at the liquid-solid interface. [32]

2.2.2 Nanowire crystal structure

Core GaAs NWs are reportedly found to have mixture of wurtzite (WZ) and zinc blende structure but when Sb is incorporated in the structure it becomes all zinc blende (ZB). In nanoscale hexagonal WZ structure is the stable one in GaAs for thin NWs, but it can revert back to cubic ZB structure for thicker wires. [4]. NWs that are used for μ -PL throughout this thesis exhibit ZB structure because of the 70-100 nm thick GaAs core and presence of Sb in the shell.

2.3 Photoluminescence of GaAs(Sb) Nanowires

With a unique density of electronic states due to two dimensional confinement, NWs exhibit significantly different optical properties as compared to the bulk material. In particular, the III-V NWs stand out with their exceptionally high electron mobility and possibility of low lasing threshold. The small footprint of the nanowire in conjunction with the ability to grow axial and radial configured structure enables efficient alloy bandgap engineering.

Photoluminescence is a spectroscopy technique providing information on bandgap, crystal structure and defects of semiconductor materials. Following presents an overview on the photoluminescence study of GaAs-GaAs(Sb) core-shell NWs.

2.3.1 Variation in low temperature (4K) μ -PL of ensemble of GaAs-GaAsSb heterostructured NWs for different Sb compositions

The effects of GaAsSb inserts and comparison with core-shell NW on the optical properties of GaAs/GaAsSb heterostructured nanowires are reported. Twins are found along the sides of the inserts which affected the μ -PL. [33] In our group 4K photoluminescence (PL) of GaAs-GaAsSb NWs of axial configuration exhibited a red shift to 1.2 eV with increasing Sb incorporation up to 4 at.%. [34]

2.3.2 Intensity dependent μ -PL- Type I & type-II band alignment in heterostructures

A blue shift in μ -PL peak energy with laser power intensity is reported to be characteristic of type-II transitions in the material and no shift in μ -PL peak energy with changing laser power intensity indicated type-I transitions in the material. [33] The blue-shift originates from separation of charge carriers in a type-II system that induces electrostatic potential (repulsive Hartree potential) and thereby causing band bending at the interface with increased laser intensity. Confinement of the carrier under the influence of band bending elevates the ground state energy of the electron relative to the flat band case resulting in a blue shift in PL peak energy. The resulting shift is determined in a competition between these two processes. [35] Type-I band alignment has been reported to associate with relatively high PL intensity of the bare-core WZ NWs. Bare core ZB GaAsSb showed type-I band alignment, as ascertained from intensity dependent μ -PL. [36] In another report, incident laser power dependent spectra from the GaAsSb related PL peak showed type II band alignment with the upper GaAs barrier containing thin ZB GaAs segment. [18].

2.3.3 Temperature dependent μ -PL

The low-temperature emission from GaAs-AlGaAs core shell NWs are found to be strongly enhanced compared with that observed in bare GaAs nanowires. The temperature-dependent μ -PL peak energy of core-shell nanowires are seen to be different from that observed in bulk GaAs, and the PL is reported to rapidly quench above 120 K. [37] In another report [38], the integrated intensity are found to rapidly decrease with increasing temperature, especially above 80 K for axial GaAsSb and the shift in peak energy could be fitted using the phenomenological Varshni equation. [39]

$$E_g(T) = E_g(0) - \frac{\alpha T^2}{\beta + T}$$

where α and β are fitting parameters characteristic of a given material. β is approximately close to Debye temperature in $^{\circ}\text{K}$, and α is an empirical constant. [39]

2.3.4 Single nanowire μ -PL

A process to perform μ -PL spectroscopy on single NWs is explained where the NWs were scrapped off from the substrate and then dispersed onto a patterned Si substrate to an average density of $0.1 \text{ NW}\mu\text{m}^{-2}$. [18] Single WZ GaAs nanowires are reported to have free exciton emission at an energy $\sim 29 \text{ meV}$ higher in comparison with the free exciton emission energy in ZB GaAs. Temperature dependent μ -PL showed small red shift with increasing temperature. [40] Temperature dependent study on a core-shell (Al)GaAs single NW is reported to deviate from bulk GaAs band gap but suggested presence of non-radiative centers by quenching at 120K. [37]

CHAPTER 3

Methodology

In this chapter descriptions of the equipment that were used to carry on μ -PL are given. The related processes are outlined and explained for μ -PL measurement of ensemble of NWs and single NWs. An associated work on the development of the optical system to make it more user friendly are described at the end of this chapter.

3.1 Equipment and Tools

A schematic of the μ -PL set up used in this experiment is shown in Fig. 8.

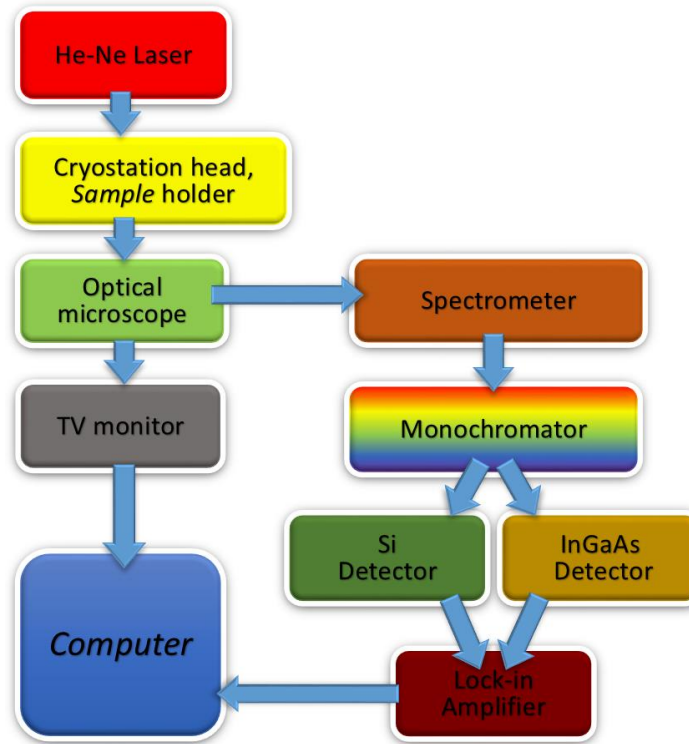


Figure 8. Schematic showing the μ -PL set up.

Fig. 9 shows the experimental setup for low temperature μ -PL measurement in the optics lab. A custom made μ -PL set up has been installed comprising of low vibration optical cryostat from Montana Cryostation interfaced with a fiber coupled confocal microscope from Horiba Jobin Yvon, Inc. It is equipped with a charge coupled device and a color TV camera that enables

simultaneous viewing of the sample and the laser spot. 'Synergy' software is used for data acquisition for PL measurements. The NW's are excited using 633nm He-Ne laser with a maximum power density of 35.0 mW. The laser focused on few (2~4) NWs using Infra-Red capable objective lens (50X, NA=0.9 Zeiss optics). The PL from the NWs is collected by the same lens, dispersed by a spectrograph (Horiba iHR 320). The spectra is collected by either Si photo-detector in the range of 700~1150 nm or InGaAs detector in the range of 800~2950 nm, which are attached to the two ports of the monochromator. An attached external lock in amplifier is used to acquire signals from the detector.

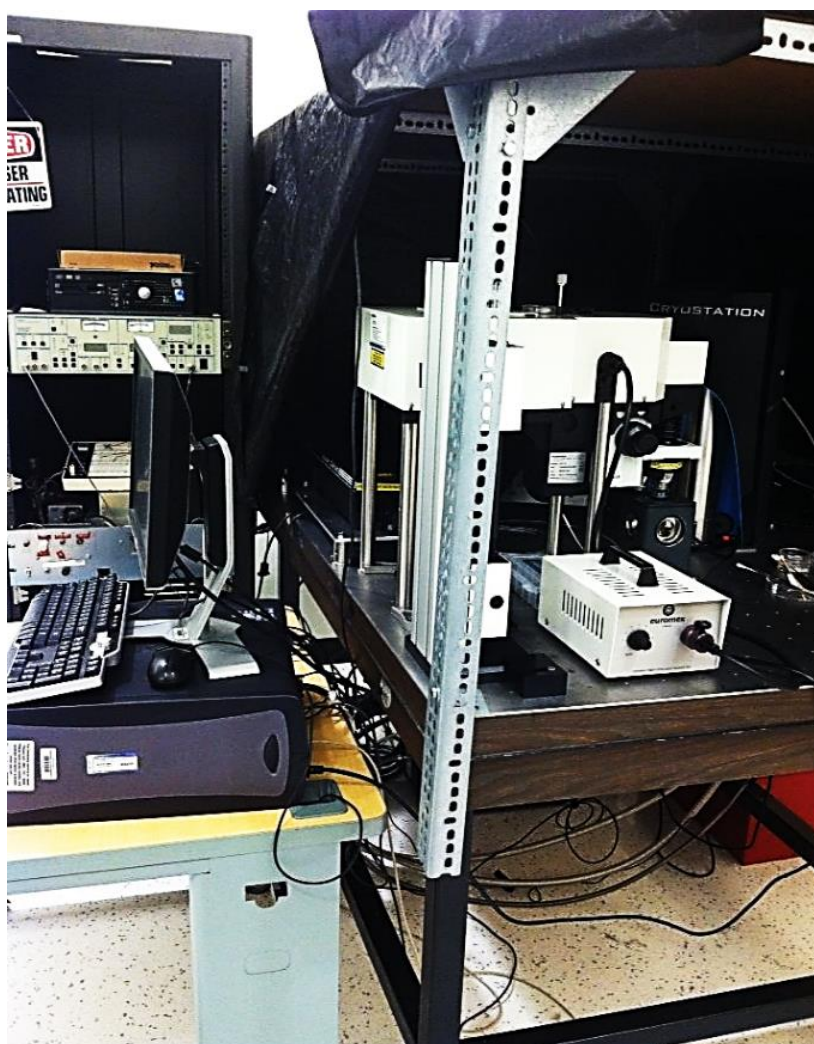


Figure 9. μ -PL setup in the Optics Lab.

3.1.1 Laser

A 633nm non-polarized He-Ne laser was used as the excitation source for the μ -PL measurement of NWs with a maximum output laser power density of 35.0 mW.

3.1.2 Optical microscope

A fiber coupled confocal microscope from Horiba Jobin Yvon, Inc. was used to simultaneously focus the laser on the NWs and getting the PL emission. A charge coupled device and a color TV camera that are attached to it enabled simultaneous viewing of the sample and the laser spot. Three different objective lens were used namely 10x (non-IR, working distance 10 mm), 50x (non-IR, W.D. 0.5mm) and 50x (IR, W.D. = 5.0mm). The long working distance infra-red capable 50x lens was the most generally used.

The size of the laser spot was more accurately measured by focusing the laser on the bulk sample at its maximum intensity for a long period of time (>1 hour) until the NWs get melted. Then the diameter of the melted region is measured in SEM. For IR-50x lens, the diameter of the spot is found to be $\sim 7\ \mu\text{m}$. Figure 10 shows a typical laser spot on the sample as seen under the optical microscope. The small dots in the image show the top of the NWs and the small lines represent few NWs that are possibly broken due to handling.

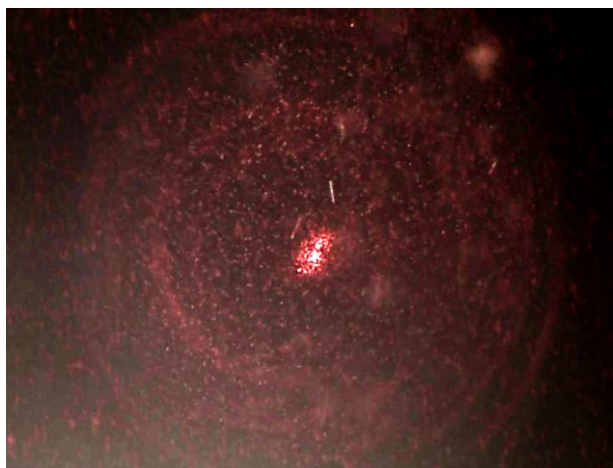


Figure 10. Laser spot on the sample.

3.1.3 Cryostation

The sample was taken to 4K using the cryostation. A cutting edge low vibration optical cryostat from Montana Cryostation was installed. It is comprised of the sample mounting chamber, compressor, mechanical pump, and the central unit. It uses helium as the cooling fluid and can practically reach up to 3.4K with a stability of 2 mK.

3.1.4 Monochromator

Monochromators are used to detect spectral lines and measure their wavelength or intensity. Once the PL from the NWs is collected by the confocal objective lens of the microscope, they are dispersed by a monochromator (Our system was installed with Horiba iHR 320 system). This is a high resolution monochromator which uses a diffraction grating at the input to split light into its component wavelengths. In other words, it works as a high refractive index prism. The single component wavelength is then allowed to transmit to the detector.

3.1.5 Detector

Two types of detector were used in this research namely- Si detector and InGaAs detector. Both are single channel detectors that only detect the intensity of one wavelength at a time. The two detectors are attached to the two ports of the monochromator. The InGaAs which is cooled with liquid nitrogen has near infra-red (NIR) detection capability while the Si detector does not. The spectra as dispersed by the spectrometer is collected by either Si photo-detector in the range of 700~1150 nm or InGaAs detector in the range of 800~2950 nm. An attached external lock in amplifier is used to get usable signals from the detector.

3.1.6 Lock-in amplifier and chopper

A lock-in amplifier is used to extract usable signals from the detector. It amplifies the noisy signal obtained from the detector and can reliably separate the signal out of the noise. In

combination with the lock-in amplifier is an optical chopper. Its frequency that serves as a reference signal to the lock in amplifier as well as modulates the intensity of the laser beam which in return also prevents the sample from burning out. In this work SR540 low jitter optical chopper was used. Two anodized aluminum blades are used having 5/6 slot blade for frequencies up to 400 Hz, and a 25/30 slot blade for frequencies up to 3.7 kHz.

3.2 Sample Preparation and Experimental Method

3.2.1 NW samples

The NWs typically have a total diameter of 150-250 nm and 2-4 μm in length, with shells typically having thickness of 50-70 nm. The structure is zinc blende (ZB) and wurtzite (WZ).

3.2.2 μ -PL of ensemble of NWs

Bulk samples as grown in MBE are cut into smaller pieces and loaded on the stage of the cryostation sample holder. The cryostation is then turned on to cool the sample at 4K temperature or it is done at room temperature. The other equipment namely lock-in amplifier, monochromator, and etc. are also turned on before doing the μ -PL scan. The laser is focused on the sample using the confocal microscope and the data is taken using Synergy software on the computer.

3.2.3 μ -PL of single NWs

NWs from the bulk sample are taken into methanol solution through ultra-sonication and then deposited on a substrate to carry on μ -PL on a single, isolated NW. The sonication time is found to vary from sample to sample and is believed to be dependent on various parameters like NW density, height, diameter, and of course, its adherence capability to the substrate on which it has been grown. Also, the amount of solvent taken plays a major role in sonication. In general, it takes 20-90 minutes to get all the NWs in to the solution. It is very important to make the timing

as precise as possible so that all the nanowires are just taken out of the sample. That is why the sample was continuously monitored during sonication. Underdoing sonication means less availability of NWs for doing PL and overdoing sonication causes the NWs in the solution to get broken. Figure 11 shows different conditions of the NWs after sonication as seen through the 50x objective lens of the optical microscope that is integrated with the μ -PL measurement system.

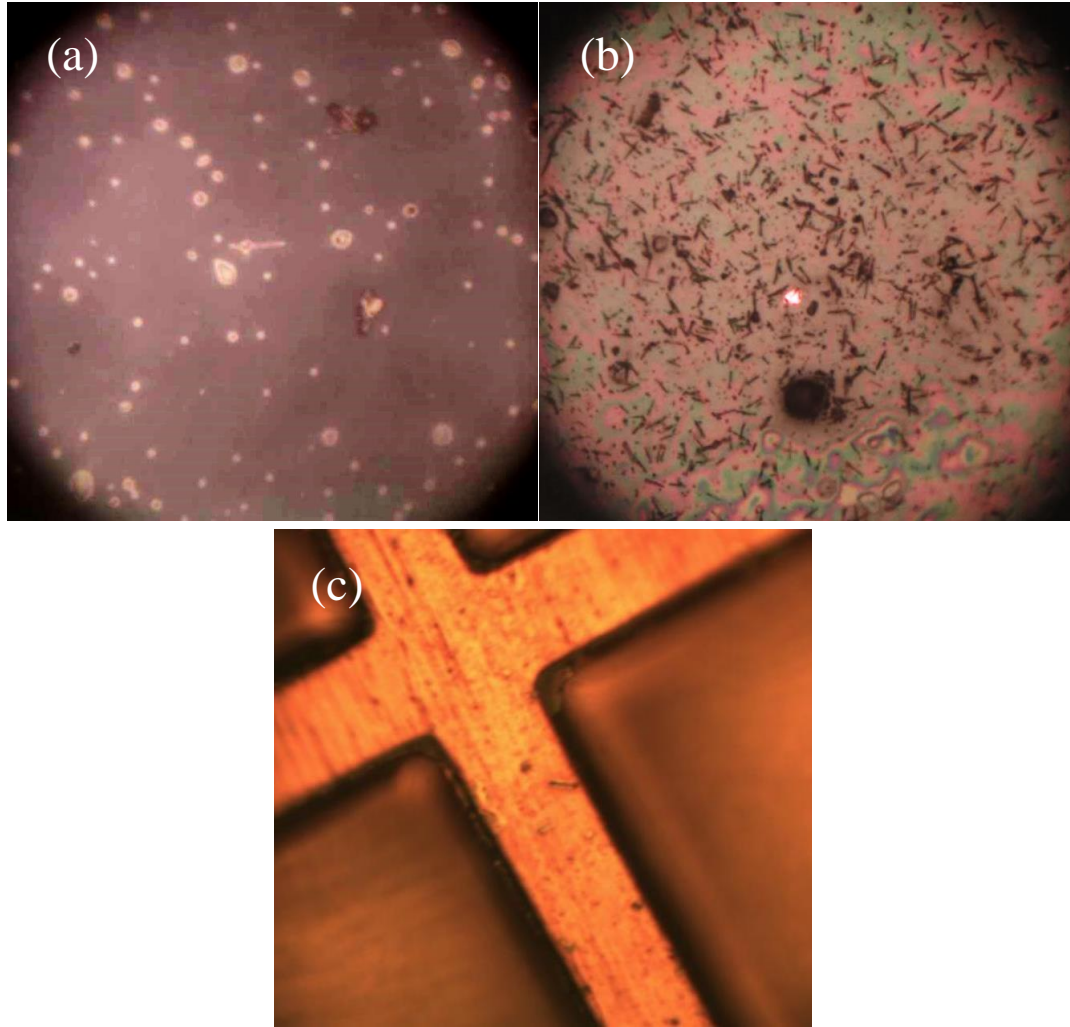


Figure 11. Optical micrographs of NWs deposited on substrate after sonication. (a) very few nanowires over SiO₂ substrate due to underdoing of sonication, (b) large number of broken NWs and pile ups due to overdoing of sonication, deposited on p-type Si substrate, and (c) single NW deposited on TEM Cu mesh.

The ongoing practice is to disperse the NWs on transmission electron microscopy (TEM) Cu-grid instead of bulk Si substrate or SiO₂ substrate because of two reasons- it will give us the exact information on the characteristic μ -PL of a single NW and also TEM can be done on the same NW. The second reason is to avoid any unwanted peak during μ -PL measurement that may appear from the substrate itself. Figure 12 shows SEM image showing isolated NWs dispersed on SiO₂ substrate and on Cu grid, and the bulk sample substrate after sonication with no NWs.

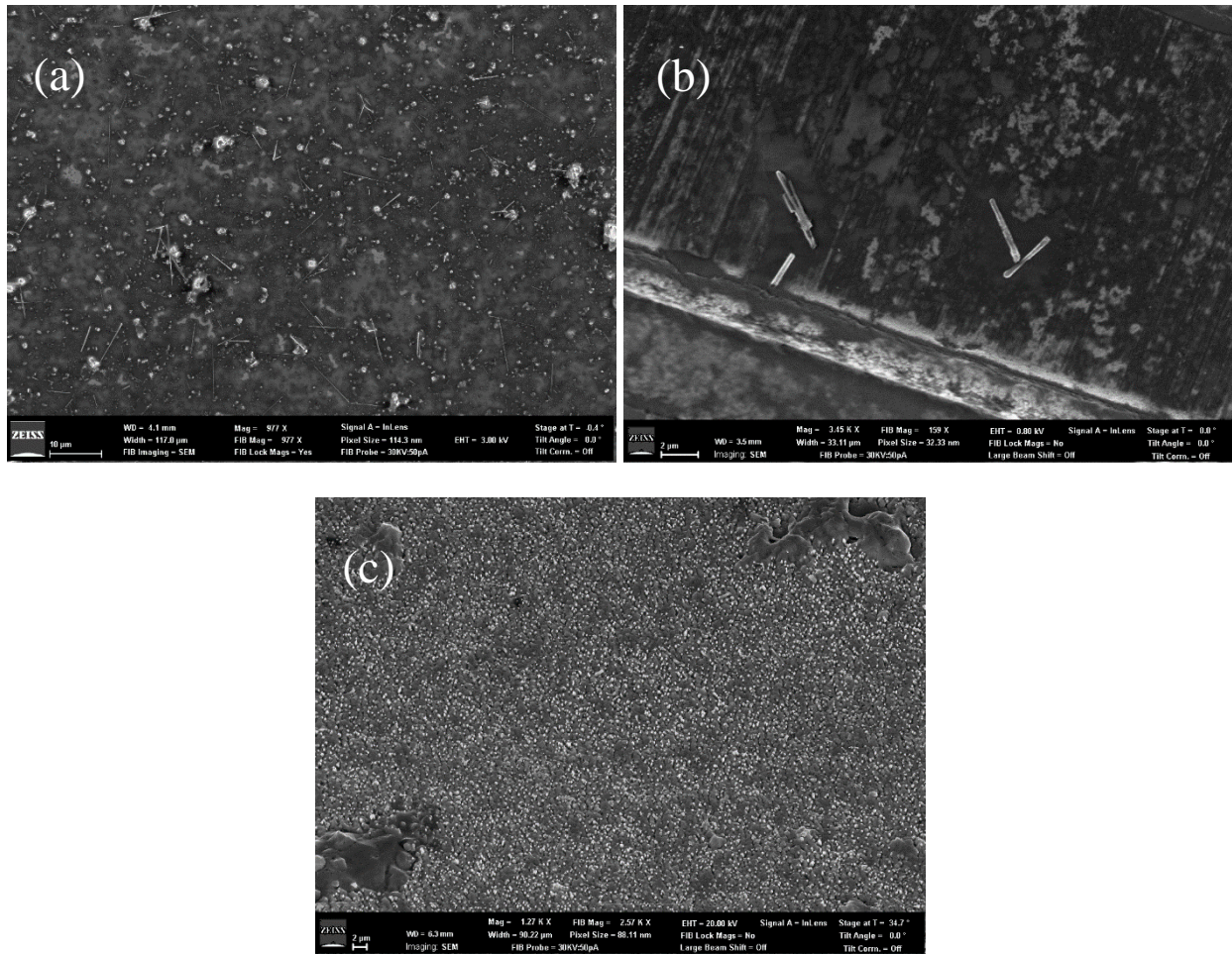


Figure 12. NW precipitate on (a) SiO₂ substrate and (b) Cu grid after sonication. (c) p-type growth substrate after sonication (NWs are not observed).

3.3 Development of the Optical System Setup

Once the sample is loaded in the cryostation chamber, there is no way the position of the sample can be changed without opening the window. Therefore there was no way the sample could be positioned on the stage at 4K which was quite inconvenient. For ensemble of NWs it could still work since the NWs were available at high, uniform density all over the substrate so the laser almost always fell on top of the NWs. But since the transition from ensemble of NWs to single NW, it became extremely inconvenient because the laser might not fall on the NW. Attaching the nanoscale piezo-positioners to the stage would be an expensive project to take in. Therefore, an external mechanical setup was installed that enabled the entire optical microscope set-up to position itself at the nanoscale so as to focus the laser on the exact NW, instead of moving the sample on the stage. This simple attachment greatly enhanced flexibility in operating the system and enabled μ -PL measurement on single NW very efficiently. Figure 13 shows the sample inside the cryostation chamber, and the external attachment that has been developed.

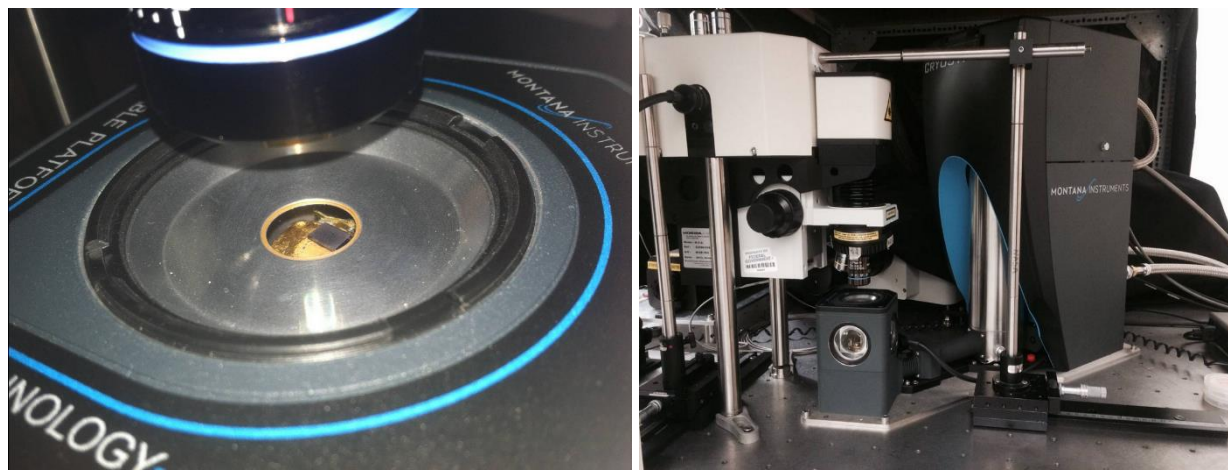


Figure 13. (a) Sample placed inside the optical cryostation chamber. (b) Confocal microscope with the external mechanical nano-positioner.

CHAPTER 4

Results

Introduction

Rigorous μ -PL experimentation have been carried out on different types of GaAsSb(N) samples under different experimental set up and conditions. The main variables are-

- Material (Composition of the material itself, structure of the material)
- Sample type (Bulk, single or ensemble of NWs)
- Laser power intensity (For intensity dependent μ -PL)
- Temperature (Room temperature low temperature, or temperature dependence)
- Detector type (Si detector or InGaAs detector)
- Objective lens (Resolution, IR or non-IR)

Other variables include scan speed, number of scans, chopper frequency, lock-in amplifier sensitivity etc. Unless otherwise stated, the incremental scan speed and chopper frequency were kept invariant at 0.1s and 54 RPM, respectively for almost all the samples. Numerous samples were examined among which only the very important or representative ones are going to be presented in the following section. First the results on low temperature (4K) μ -PL of core-shell GaAs-GaAsSb samples of different Sb compositions are presented followed by intensity dependent μ -PL and temperature dependent μ -PL on selective few samples. Then the differences in μ -PL spectra observed for the core-shell versus double shell (i.e. core-shell with passivation layer) GaAs-GaAsSb NWs are presented SEM images are taken for all of the samples that show the details about the NWs morphology but they are not explained here in detail since that is not the focus of this thesis. Also, results on μ -PL with different experimental set ups and variables are briefly presented towards the end of this chapter.

4.1 Variation in Low Temperature (4K) μ -PL of Ensemble of GaAs-GaAsSb Core-Shell Nanowires for Different Sb Compositions

Figure 14 shows the normalized μ -PL spectra of core-shell nanowires at 4K for different Sb compositions. All these data are obtained using the InGaAs detector with the IR-50x objective lens. The PL spectra of the GaAsSb nanowires are characterized by two major sets of bands, one at a higher energy (1.37 eV – 0.93 eV) and the other almost half this energy (0.67-0.48 eV). It is to be noted that with increasing Sb composition from 1 at.% to 26 at.%, the number of peaks that can be resolved, particularly in the higher energy spectral band increases, along with red shift and peak broadening.

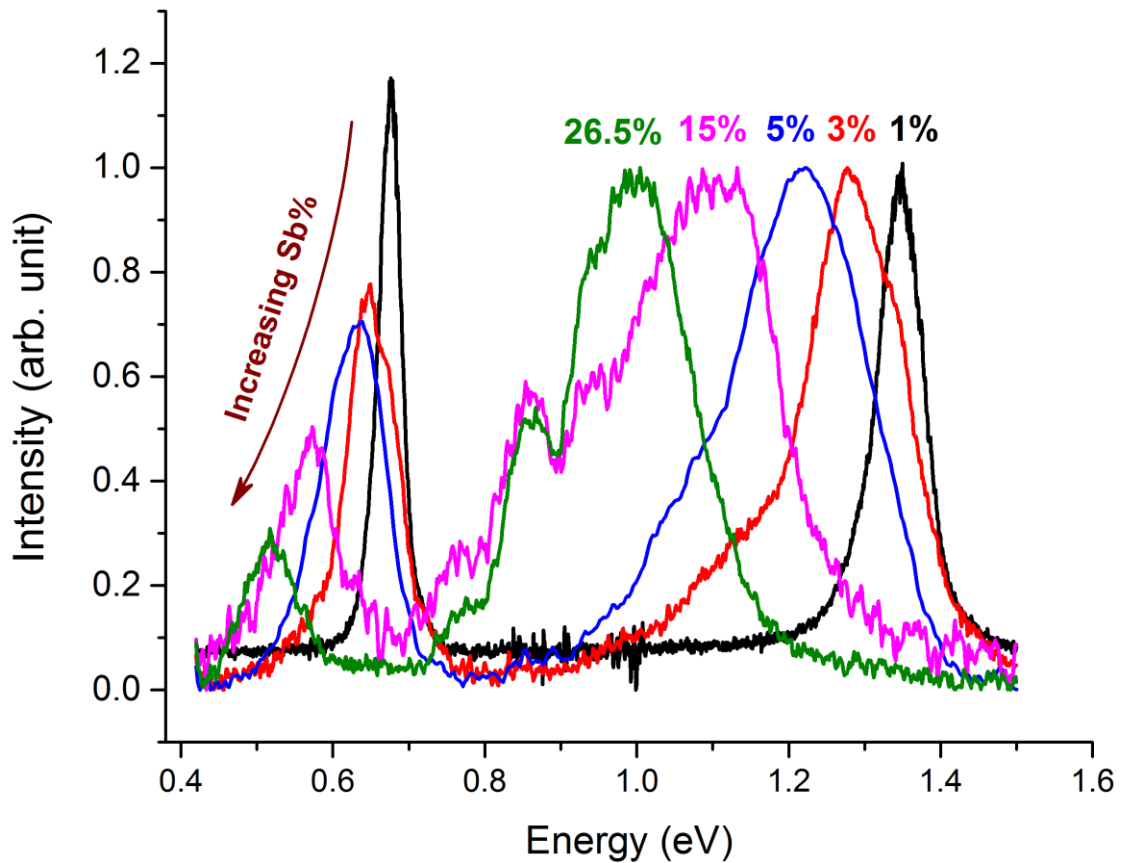


Figure 14. Normalized low temperature (4K) μ -PL of ensemble of GaAs-GaAsSb core-shell nanowires for different Sb compositions.

Figure 15 shows the possible breakdown of peaks for every sample. Total of six peaks are Gaussian fitted for each of the samples having Sb-1 at.%, Sb-3 at.%, and Sb-5 at.%, each having three peaks in the lower energy set (0.67 - 0.48 eV), and three in the higher energy set (1.37 eV – 0.93 eV). On the other hand total of eight peaks are fitted for each of the samples having Sb-15 at.% and Sb-26.5 at.% each, with three in the higher energy set (1.37 eV – 0.93 eV), three in the lower energy set (0.67 - 0.48 eV) and two in the mid-range (0.75 eV – 0.84 eV).

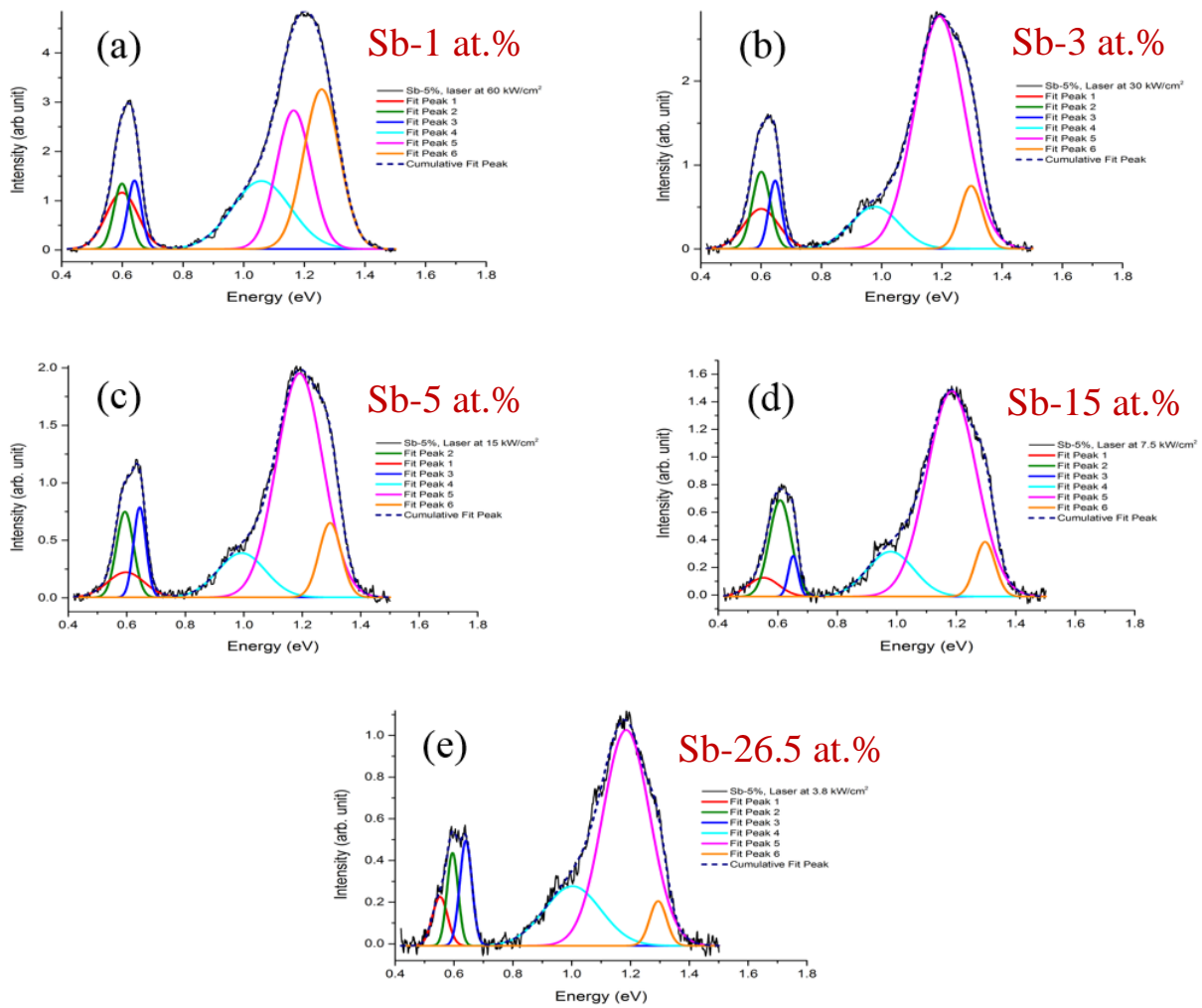


Figure 15. Multi-peak fit for μ -PL of GaAs-GaAsSb core-shell NW with (a) Sb-1 at.%, (b) Sb-3 at.% (c) Sb-5 at.% (d) Sb-15 at.%, and (e) Sb-26.5 at.% compositions.

Shifts in individual peaks are shown in Fig. 16.

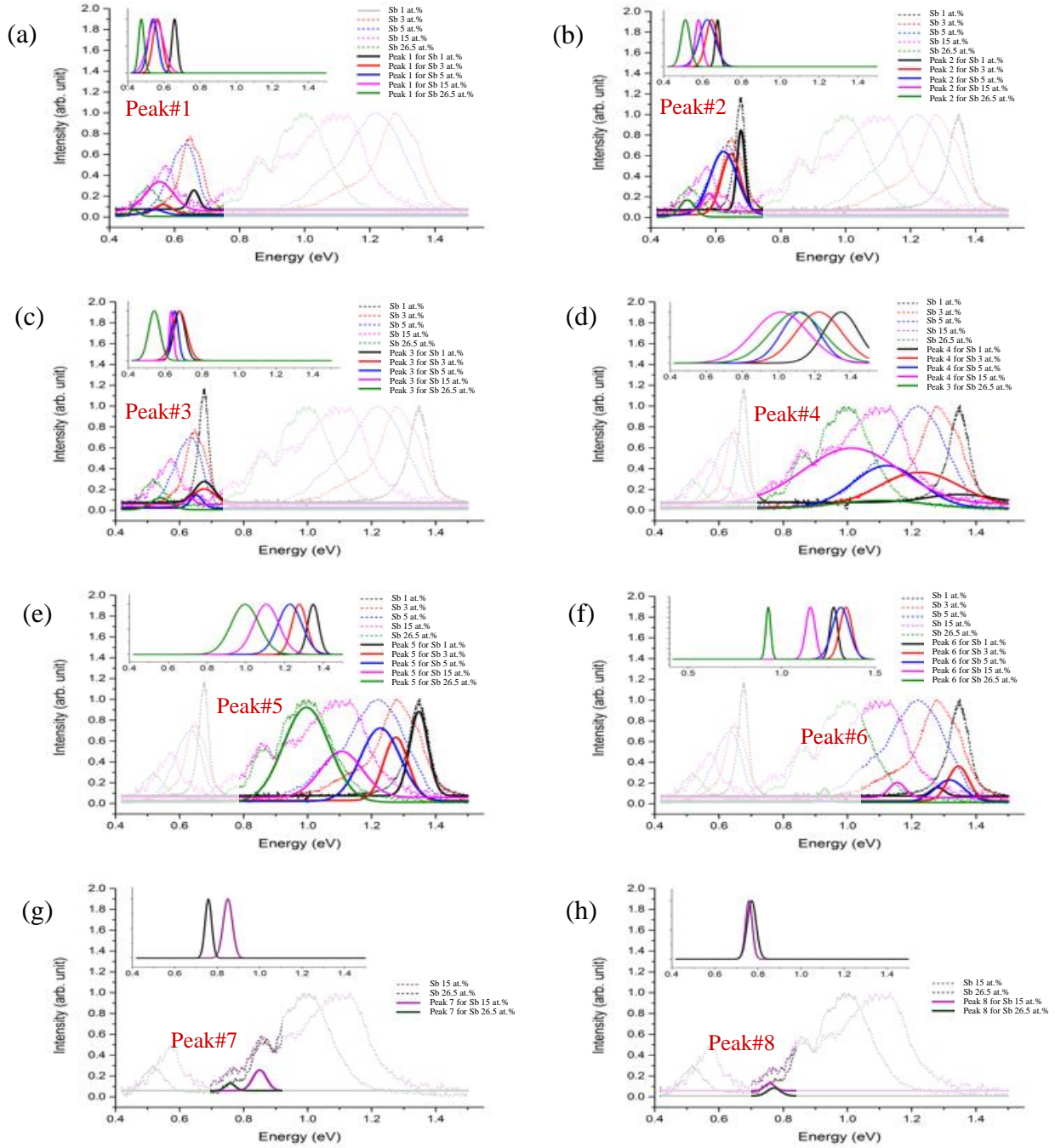


Figure 16. Gaussian fit of (a) Peak 1, (b) Peak 2, (c) Peak 3, (d) Peak 4, (e) Peak 5, (f) Peak 6, (g) Peak 7, and (h) Peak 8 for μ -PL of GaAs-GaAsSb core-shell NWs with different Sb compositions. Insets show the normalized form of the fitted peaks.

The results from the Gaussian peak fits from Fig. 16 are summarized in Table 4.1 below.

The shifts in each peak position with changing Sb composition from 1 at.% to 26.5 at.% are shown in Fig. 17.

Table 1

Change in core-shell GaAs-GaAsSb peak with Sb at.% composition

Peak	Peak range (eV)	Change in peak position with Sb composition varying from Sb-1 at.% to 26.5 at.% composition (Sb-15 at.% to Sb-26.5 at.% for peak-7 and peak-8)		Change in peak FWHM from Sb-1 at.% to 26.5 at.% composition (Sb- 15 at.% to Sb-26.5 at.% for peak-7 and peak-8)	
		Change (meV)	Nature of change	Average size (meV)	Nature of change
1	0.660 – 0.476	184	red-shifted	59.042	Broadened Or, Irregular
2	0.677 – 0.512	165	red-shifted	58.536	Broadened
3	0.677 – 0.541	136	red-shifted	61.42	Broadened Or, Irregular
4	1.348 – 0.996	352	Red-shifted	231.862	Broadened Or, Irregular
5	1.347 – 0.999	348	red-shifted	125.068	Broadened
6	1.280 – 1.102	178	red-shifted	126.244	Broadened
7	0.758 – 0.771	13	blue-shifted	50.775	Broadened
8	0.849 – 0.850	1	blue-shifted	56.9	Broadened

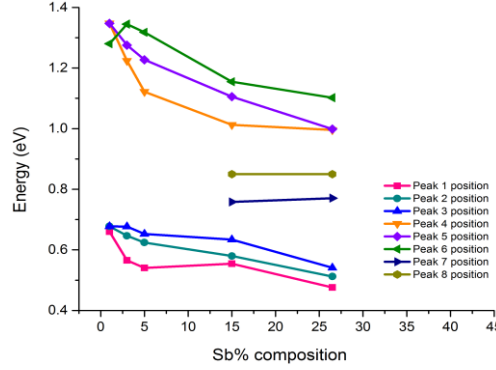


Figure 17. Shift in μ -PL peaks in core-shell GaAs-GaAsSb NWs with increasing Sb at.% composition.

The change in bandgap with Sb composition is mostly accommodated by the change in VB offset in this heterostructure which is more pronounced than in CB offset. The Type-I/Type-II nature of transitions were deduced from the peak-shift in excitation power dependent 4K μ -PL spectra as discussed in the following section 4.2. A band gap alignment is proposed for these samples based on these data which is shown in the schematic of Fig. 18. Most of the μ -PL transitions observed here are ascribed to the presence of two defect levels namely- the V_{As} defect level which is located at 0.14 eV below the CB [41], and an EL2 midgap donor level [42] or a surface defect level [43] the assignment of which (L) is uncertain. The position of the reported EL2 level is determined from μ -PL and is found to vary from 0.51 eV to 0.68 eV but the presence of this level at low temperature is still under debate [44] [45]. The surface defect level, which is expected to pin the Fermi level (E_F) below the CB of $GaAs_{1-x}Sb_x$, is reported to vary as a function of Sb composition in the relation of $E=0.70-0.192x$ [43]. The calculated range of E_F for Sb-1 at.% to Sb-26.5 at.% according to this expression is found to be 0.70-0.65 eV, which appears to be slightly higher than the values obtained from the experimental investigation on μ -PL in this thesis. The characteristic of this level is not quite clear yet, but it is always found to be near the middle of Type-II transition.

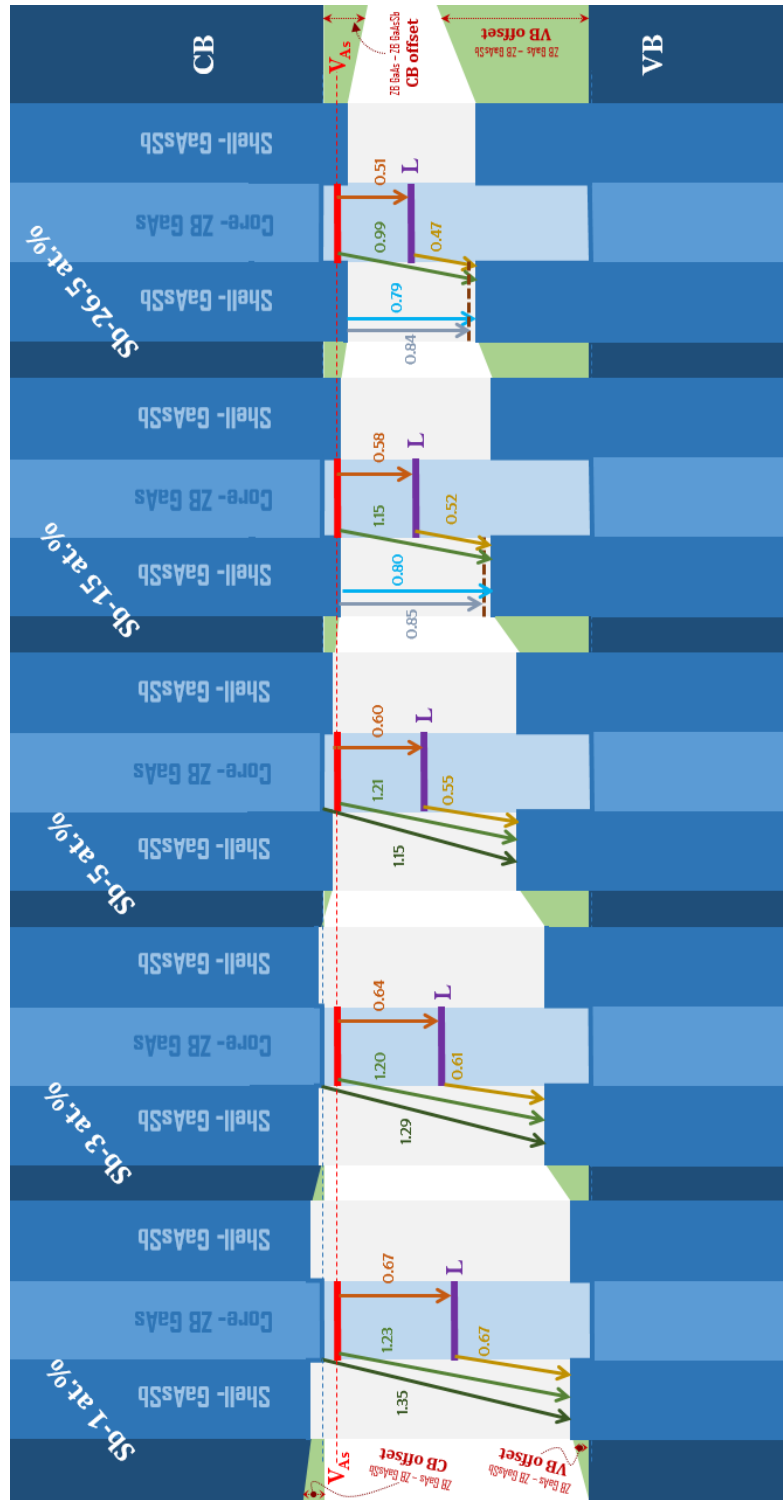


Figure 18. Shift in PL peaks in core-shell GaAs-GaAsSb NWs with increasing Sb at.% composition.

SEM images show high and uniform density of NWs over the samples with over 99% vertical alignment. Densities lie in the order of $5 \times 10^8 \text{ cm}^{-2}$ and NWs are typically 160-270 nm in diameter and 3-5 μm in length. Figure 19 shows typical NWs on the bulk, both core and core-shell NWs. Figure 20 shows the shape and morphology of single NWs as it changes with Sb at.% composition which depicts the enhanced strain associated with increased Sb incorporation.

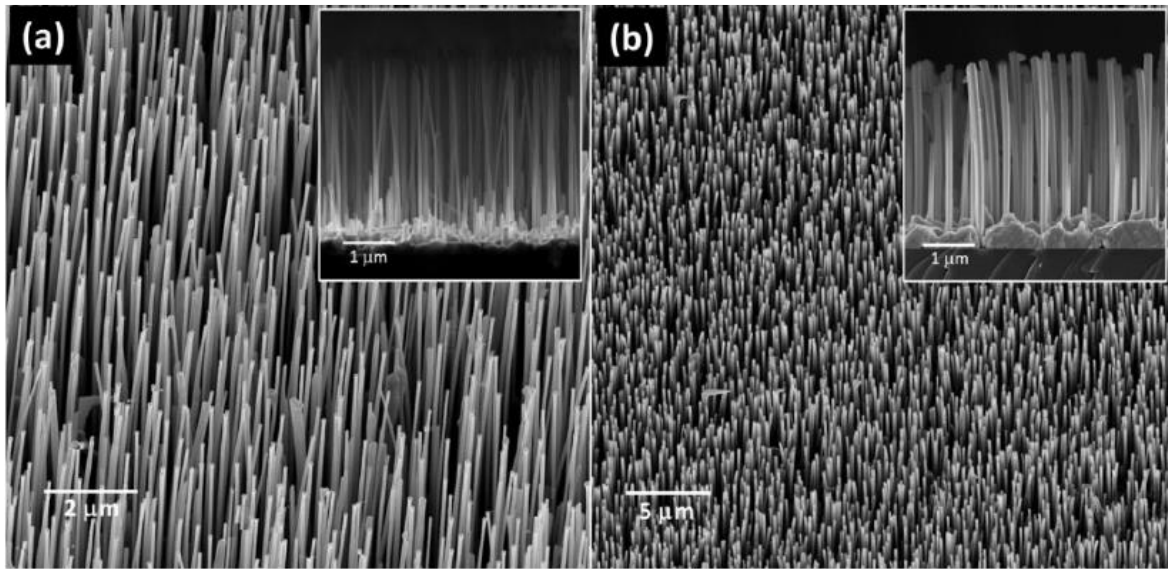


Figure 19. (a) Core GaAs nanowires and (b) core-shell GaAs/GaAsSb nanowires. The insets show the respective side views of the NWs.

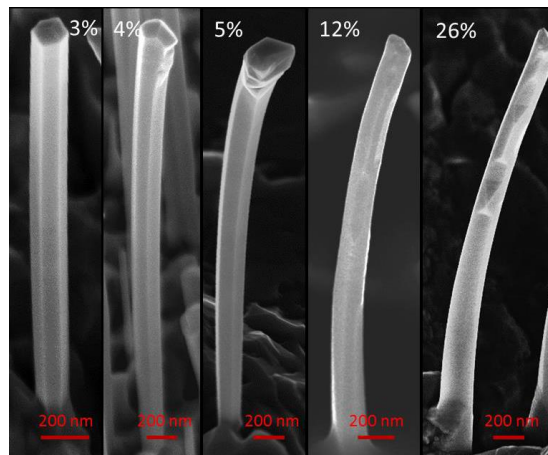


Figure 20. SEM images of single GaAs/GaAsSb core-shell nanowires for different Sb at.%.

4.2 Intensity Dependent μ -PL of Ensemble of GaAs/GaAsSb Nanowires

Intensity dependent μ -PL of ensemble of NWs were carried out on various type of samples, both at room temperature and low temperature and using both detectors (Si and InGaAs). But only a representative sample is presented here in detail.

Figure 21 illustrates the low temperature intensity dependent (4K) μ -PL of GaAs-GaAsSb core-shell NW with Sb-5 at.% composition. The data was obtained using InGaAs detector and 50x-IR objective lens.

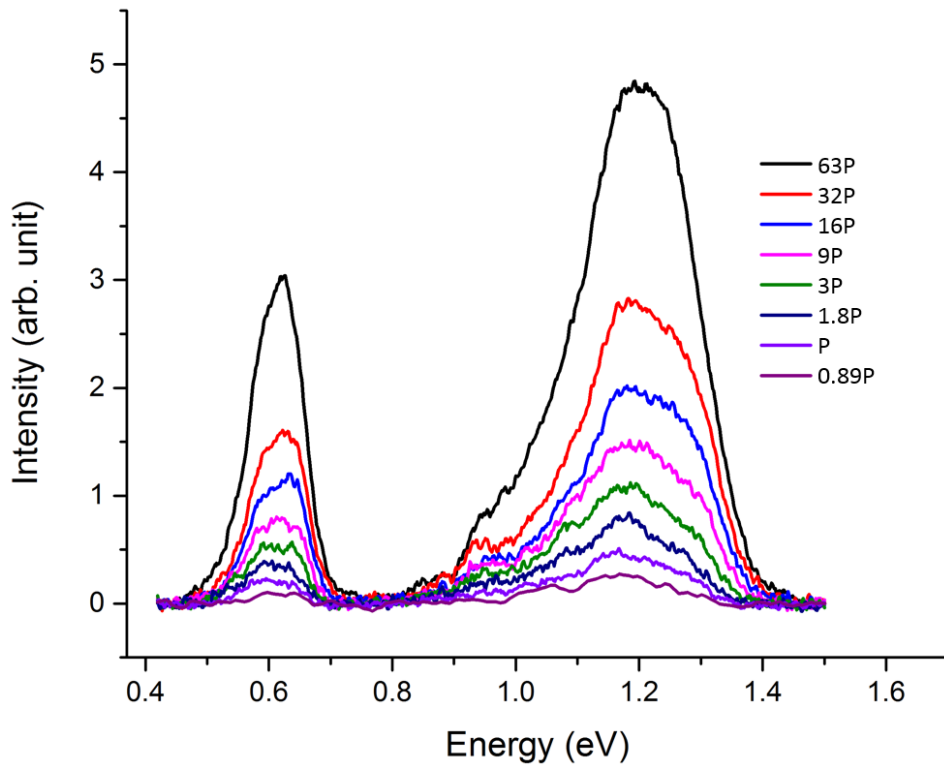


Figure 21. Low temperature (4K) intensity dependent μ -PL of GaAs-GaAsSb core-shell NW with Sb-5 at.% composition.

To understand the direction of shift in the peaks with increasing laser power, each curve is multi-peak (six peaks in each) fitted using Gauss method as before and shown in Fig. 22. The fitted multi-peaks for the first five curves with high laser intensities (3.8 – 60 kW/cm²) have less

than 2% standard error while the μ -PL curves for the low laser intensities ($0.48 - 1.9 \text{ kW/cm}^2$) are not fitted because they incorporate much noise that is associated with more than the acceptable standard error.

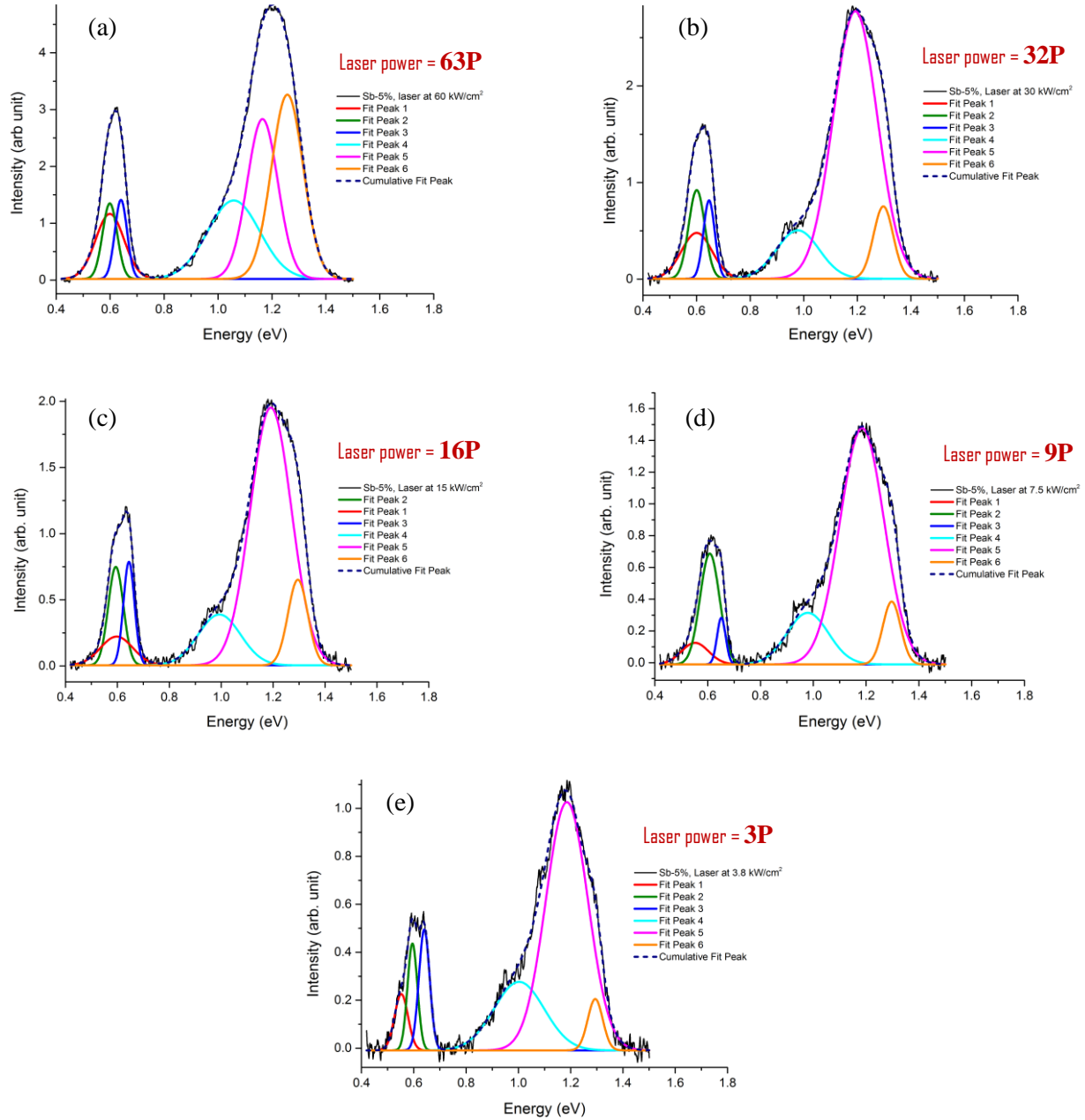


Figure 22. Multi-peak fit of low temperature (4K) intensity dependent μ -PL of GaAs-GaAsSb core-shell NW for different laser power intensities- (a) 63P, (b) 32P, (c) 16P, (d) 9P, and (e) 3P.

The change in peak position for each peak are shown in Fig. 23. Some peaks showed blue shifts while others showed red shifts. The origin and significance of these shifts are explained in the literature review (refer to section 2.3.2). [35]

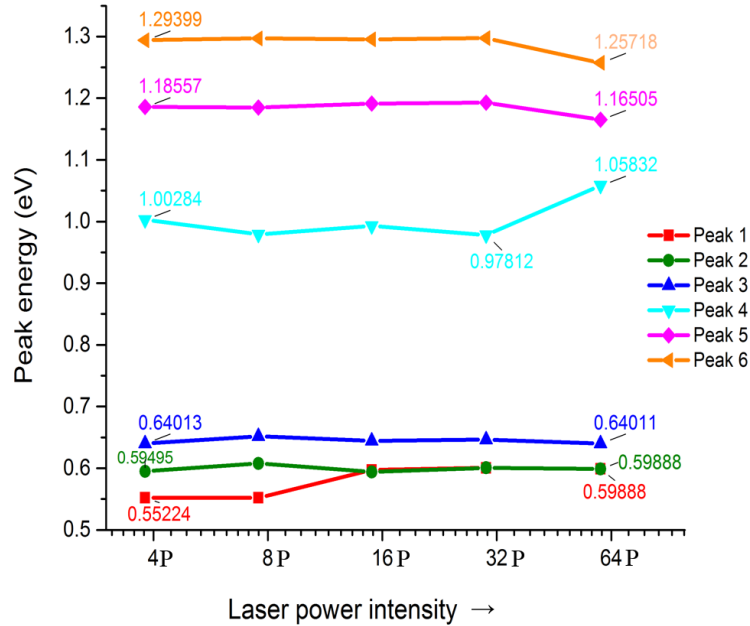


Figure 23. Change in peak position with multi-peak fit of low temperature (4K) intensity dependent μ -PL of GaAs-GaAsSb core-shell NW for different laser power intensities. The energy in horizontal axes are in $\log(2)$ scale.

To understand the nature of the two additional peaks that show up in the mid-energy range (0.75 eV – 0.87 eV, refer to Fig. 14 for Sb-15 at.% and Sb-26.5 at.%) in core-shell GaAs-GaAsSb samples with higher Sb composition, intensity dependent 4K μ -PL of GaAs-GaAsSb core-shell NW with Sb-12 at.% composition is shown in Fig. 24. Details of the curve fitting are not shown in here. Note the additional peak for this sample at around 1.33 eV which is believed to be due to defects and going to be explained later in the chapter.

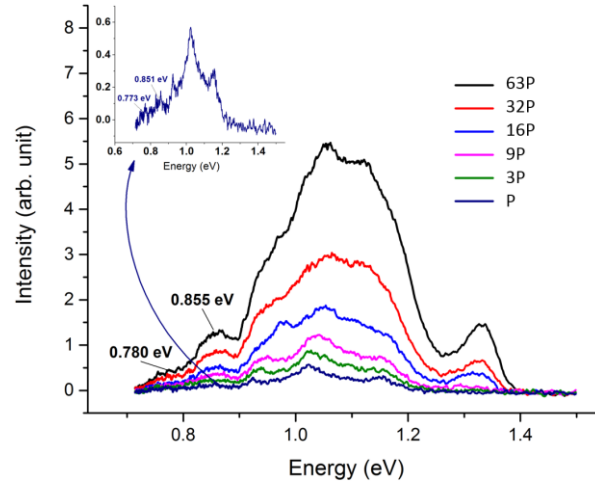


Figure 24. Low temperature (4K) intensity dependent μ -PL of GaAs-GaAsSb core-shell NW with Sb-12 at.% composition.

Instead of fitting several peaks, the intensity dependent μ -PL spectra of GaAs-GaAsSb core-shell NW with 3 at.% composition were curve fitted using two Gaussian peaks for both the high energy and low energy spectral bands. The fitting is not shown but the resulting peak energies from the best curve fit are indicated in Fig. 25.

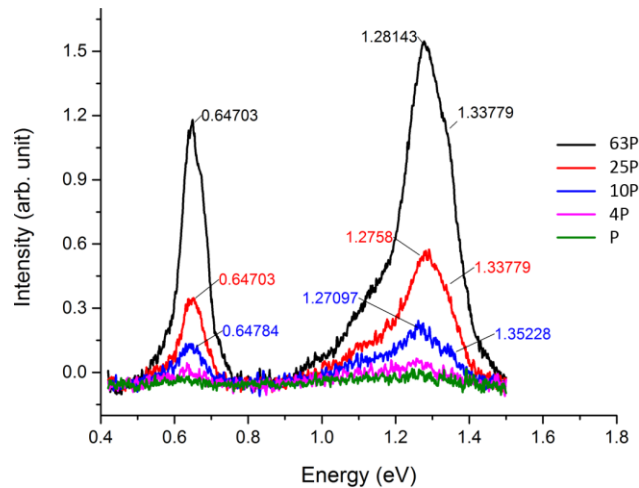


Figure 25. Low temperature (4K) intensity dependent μ -PL of GaAs-GaAsSb core-shell NW with Sb-3 at.% composition.

4.3 Temperature Dependent μ -PL of Ensemble of GaAs/GaAsSb Nanowires

Temperature dependent μ -PL of ensemble of NWs are carried out on various type of samples, ranging from low temperature (4K) to room temperature (293K) and using both detectors (Si and InGaAs). A representative sample is presented here in detail. Temperature dependent μ -PL spectra is shown in Fig. 26 for GaAs NWs with GaAsSb insert of Sb-5 at.% composition. It was taken using the Si detector with the 10x non-IR objective lens. The NW emission in this case is characterized by redshifts of ~ 315 meV with increasing temperature from 4K to room temperature and is also coupled with peak broadening. Fitting of these data are done using the phenomenological Varshni equation which shows the consistency of the results with the previous data [38] that is also presented here.

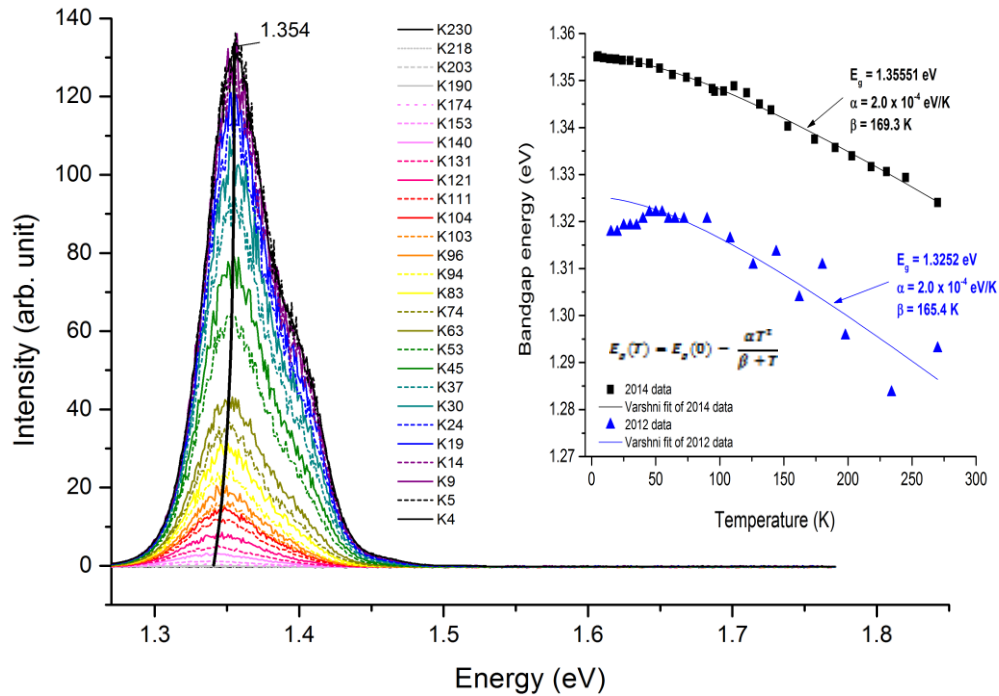


Figure 26. Intensity dependent μ -PL of GaAs NW with GaAsSb insert of Sb-5 at.% composition (2014 data). Inset shows change in bandgap energy of the first peak around 1.35 eV with temperature and Varshni fit, superimposed with previous data [38].

The Varshni expression for the temperature dependence of semiconductor band gaps is given by-

$$E_g(T) = E_g(0) - \frac{\alpha T^2}{\beta + T}$$

where α and β are fitting parameters characteristic of a given material. β is approximately the Debye temperature in °K, and α is an empirical constant. [39]

Table 2 shows the fit parameters for temperature dependence of semiconductor band gaps for the NWs as compared to bulk GaAs.

Table 2

Fit parameters for temperature dependence of semiconductor band gaps

Material	Temperature range (K)	$E_g(0)$ eV	α ($\times 10^{-4}$ eV/K)	β (K)	Ref.
Bulk GaAs	0-300	1.522	5.8	300	[46]
NW GaAsSb (2012)	0-300	1.3252	2	165.4	[38]
NW GaAsSb (2014)	0-300	1.3555	2	169.3	[38]

The low values of α and β in NWs in comparison to GaAs bulk values are indicative of less temperature dependency of PL peak energy, a desirable feature for optoelectronic devices.

4.4 Comparison of μ -PL Between Core-shell GaAs/GaAsSb and Core-shell With Passivation Layer GaAs/GaAsSb/GaAs Nanowires

A significant improvement in μ -PL intensity has been found in a GaAs-GaAsSb core-shell NW configuration with GaAs passivation layer over the shell (i.e. a double shell) than in bare core-shell NWs. Figure 27 shows the difference between low and room temperature μ -PL peak intensity of core-shell (Sb-3 at.%) and double shell (Sb-4.7 at.%) NWs. The major peak (~ 1.2 eV) of the double-shell sample at 4K is found to be 12-fold higher than that of the core-shell sample at 4K while the increase is about 5 fold at the room temperature, a great improvement in the signal.

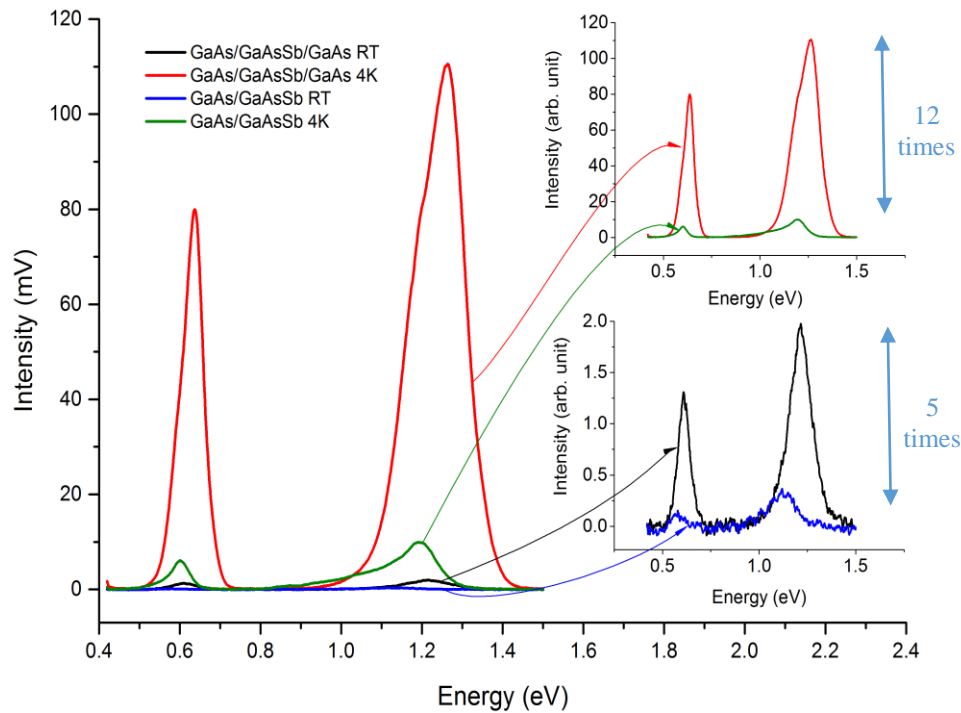


Figure 27. Intensity dependent μ -PL of GaAs-GaAsSb core-shell NW with Sb-3 at.% composition and GaAs-GaAsSb-GaAs double-shell NW with Sb-4.7 at.% composition in its GaAsSb shell. Inset shows the multifold increase in μ -PL signal between the two both at room temperature and 4K.

4.5 μ -PL of GaAs-GaAsSb(N) Nanowires

An outstanding result in μ -PL of the novel GaAs-GaAsSb(N) double shell NWs shows very small difference between room temperature and low temperature. In general the regular GaAs-GaAsSb core-shell NWs usually do not show any noticeable peak at the room temperature, or even if they do it is of very low intensity. But these nitride samples show defined peaks at even room temperature and they are closely comparable to their 4K μ -PL. Figure 28 shows the room temperature and low temperature μ -PL of core-shell GaAs-GaAsSb(N) samples in as grown. Despite the fact that nitride samples had low overall intensity, it showed only 2-5 fold increase from room temperature to 4K as compared to > 5 fold increase which is normally found in core-shell GaAs-GaAsSb NWs. Red-shift at higher temperature is observed while peak broadening is reduced as compared to non-nitride samples. These are just very preliminary results and shows great promise for NIR applications.

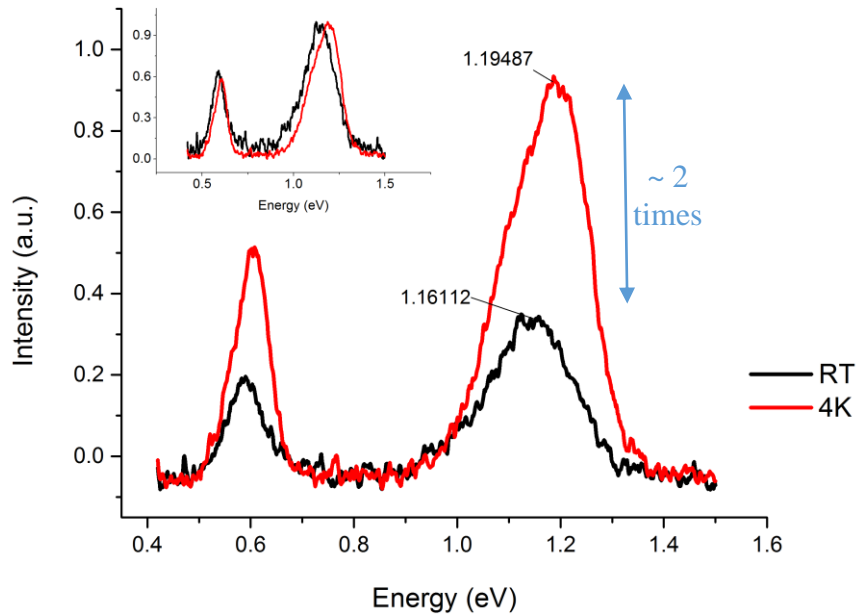


Figure 28. μ -PL of as-grown GaAs-GaAsSb(N) core-shell NW at room temperature and 4K.

Inset shows the redshift and almost identical FWHM on normalized plot of the two curves.

4.6 μ -PL of Single NWs

μ -PL from single NWs are found to show very similar results to their bulk or ensembled form and they are quite consistent. They are found to show less burning effect.

Figure 29 shows the low temperature (4K) μ -PL of ensemble of NWs on the bulk substrate and μ -PL of three different single NWs from the core-shell GaAs-GaAsSb sample with Sb-26.5 at.% composition. Four peaks are found at exactly the same emission energy of 0.78, 0.85, 0.95 and 1.01 eV which show good compositional homogeneity of the NWs in the ensemble. Also noticeable that in this case, the single NWs have higher μ -PL signal intensity than that of the ensemble of NWs, though the validity of this for all single NWs has not yet been proven.

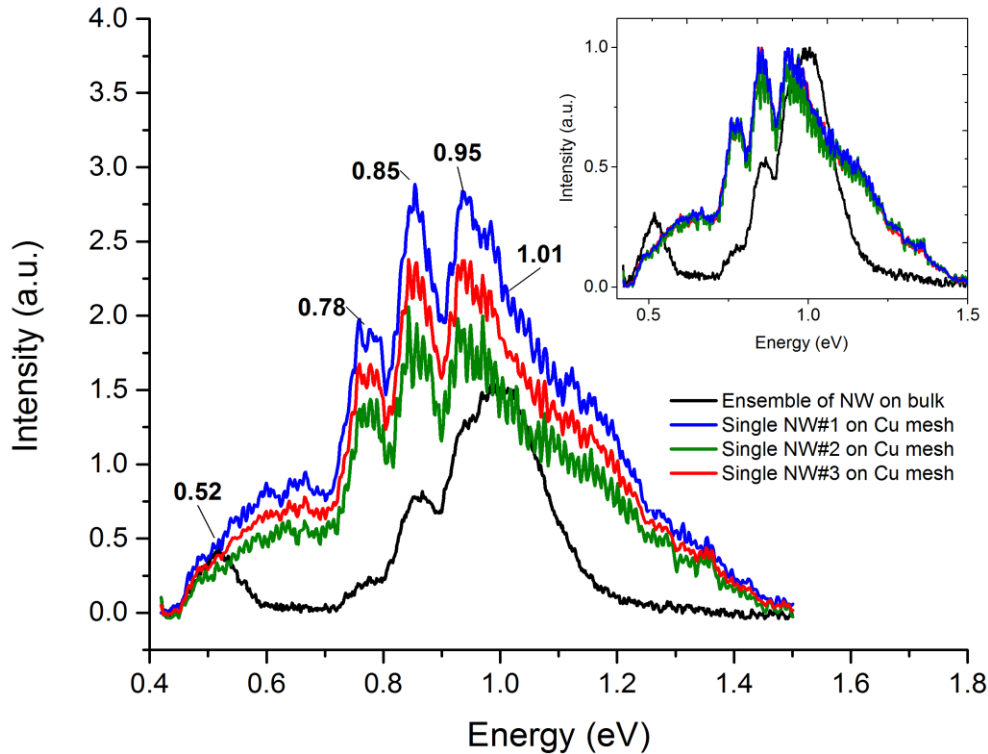


Figure 29. Low temperature (4K) μ -PL of single and ensemble of GaAs-GaAsSb core-shell NWs with Sb-26.5 at.% composition. Inset shows the normalized curves.

Single core-shell GaAs-GaAsSb(N) NWs show identical behavior as ensemble ones at both room temperature and 4K which is depicted in Fig. 30. We get room temperature μ -PL as before and the intensity is comparable to 4K. Both single and ensemble of NWs show about two-fold increase in emission intensity at low temperature than at 4K which is quite good. But it is noticeable that the overall signal intensity is decreased about 5 fold for the single NW.

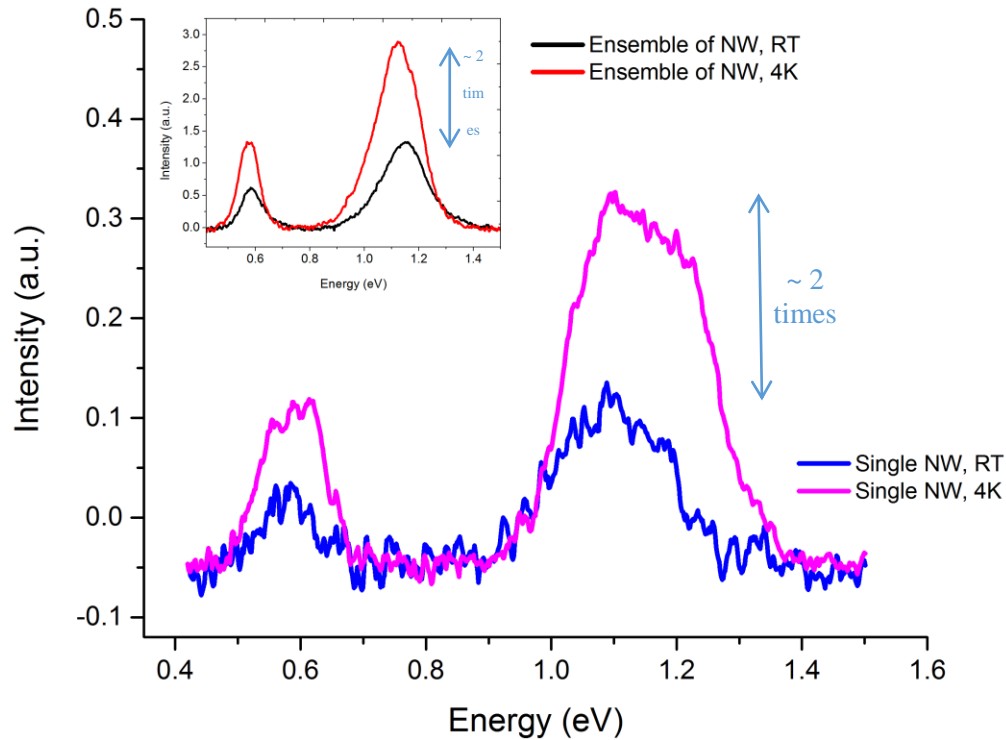


Figure 30. Room temperature and 4K μ -PL of single GaAs-GaAsSb(N) core-shell NW. Inset shows the result for ensemble of NWs for the same sample.

Due to the normally low intensity observed in single NWs, it becomes challenging to carry out intensity dependent or temperature dependent PL on them as compared to ensemble of NWs.

4.7 Effect of Experimental Variables on μ -PL

This section explains some experimental setup variables on μ -PL of NWs. This include the detector type and objective lens, chopper frequency, integration time and number of scans, focus position, effect of doing SEM before doing μ -PL, and others.

4.7.1 Detector type and objective lens

Two types of detector have been used- Si detector and InGaAs detector. The difference in the μ -PL obtained from using these two detectors are very distinctive.

4.7.1.1 Detection range. While Si detector is unable to detect in the IR region of the spectrum so unusable below 1.00 eV, InGaAs has a very wide range and it can detect signals from lower IR region up to 1.7 eV so it has been the best choice for us. The signal strength is also a lot higher with InGaAs than that of Si detector. Figure 31 shows typical μ -PL obtained using the two detectors. Note the shift in peak position which is basically due to the lower sensitivity of the Si detector towards lower energy region (<1.15 eV).

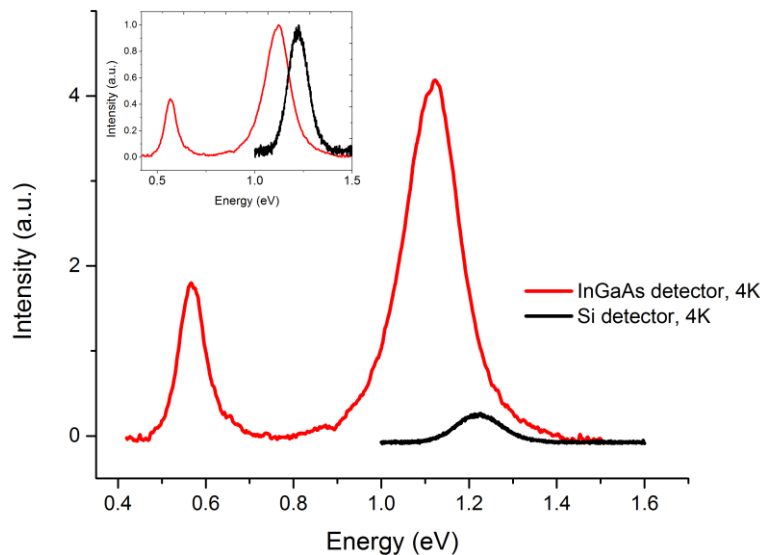


Figure 31. Low temperature (4K) μ -PL of ensemble of GaAs-GaAsSb-GaAs double-shell NWs with Sb-7~10 at.% composition. Inset shows the normalized curves.

4.7.1.2 Objective lens. A special type of objective lens is used for InGaAs detector that is transparent to IR emission (IR-50x). With Si detector normally a non-IR 10x/50x/100x objective lens is used. Using higher magnification gives much better μ -PL but at the same time it decreases the spot size concentrating the laser and making the power so high that the NWs begin to burn out which is going to be discussed later in this section. For this, usually the 50x objective lens is used which gives the best result. Using 10x gives lower signal intensity while using 100x either burns the NWs or the spot size is too small to cover the NWs, thus deteriorating the μ -PL signal. Figure 32 shows the difference in μ -PL obtained by using 10x and 50x objective lens with Si detector, and the difference in μ -PL obtained by using a test 20x-IR and regular 50x-IR objective lens.

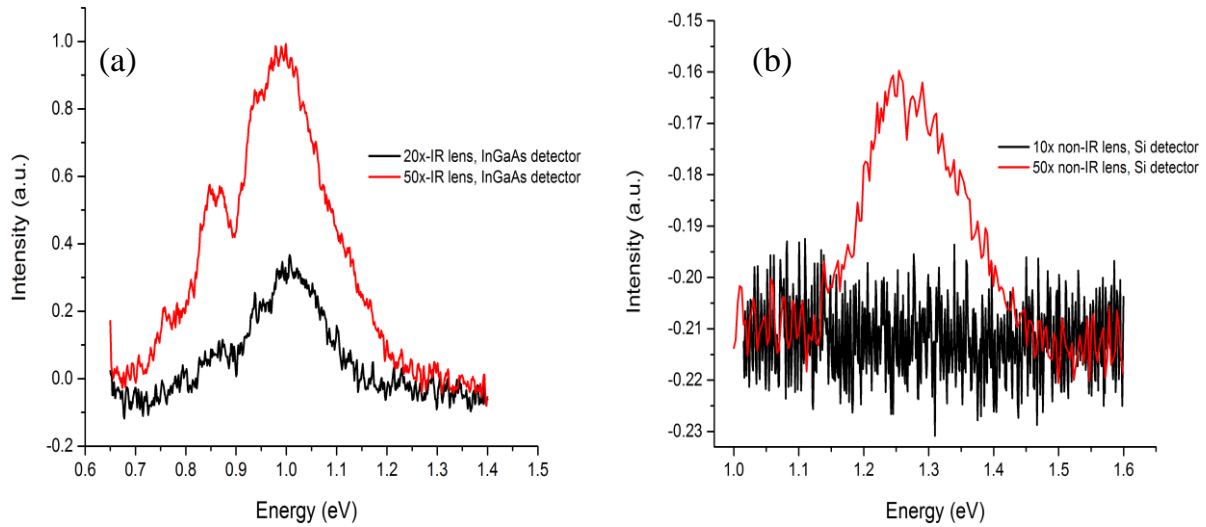


Figure 32. (a) Low temperature (4K) μ -PL of ensemble of GaAs-GaAsSb core-shell NWs, and (b) Room temperature μ -PL of ensemble of GaAs-GaAsSb(N) core-shell NWs.

4.7.1.3 Detector noise level. For the same lock in amplifier sensitivity, μ -PL obtained from Si detector incorporates comparatively lower noise than obtained from InGaAs detector and they also have less noise associated with as compared to the InGaAs detector which may make it

still useful sometimes. Figure 33 shows μ -PL of two different types of NW ensembles, scanned at 4K with Si detector and InGaAs detector separately but they have similar peak intensity and same sensitivity of 0.5 mV was used in the lock in amplifier. The level of noise with the InGaAs detector is found to be much higher than that of Si detector. Note that same sample is not used here because the overall signal intensity is normally much higher with InGaAs detector than with Si detector which appears to make up for the noise, thereby making the InGaAs detector still a better choice over Si detector. The level of noise can be attributed to many different sources e.g. thermal noise (due to carriers in constant thermal motion, macroscopic fluctuations in electrical state of system etc.), shot noise (due to random fluctuations in DC current flow), and 1/f noise (commonly associated with interface states in MOS electronics) etc. [46]

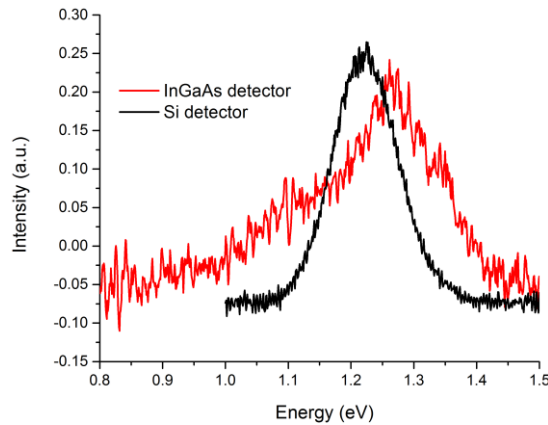


Figure 33. Low temperature (4K) μ -PL of two different NW ensembles that have similar peak intensity. Two different detector is used but the same lock in sensitivity of 0.5 mV.

4.7.2 Chopper frequency

Two different choppers were used to test the effect of chopper frequency on the μ -PL of NWs. The choppers have 6 windows and 25 windows, respectively. In terms of getting the μ -PL signal, no significant difference is found between the two of them at different speeds. However, based on the slightest difference in noise level observed, 55-75 Hz with the 25 windows chopper

are found to give the optimum result. Figure 34 shows the μ -PL of core-shell GaAs-GaAsSb(N) NW ensemble at room temperature for different chopper frequencies and a comparison between the two. The intensity are about the same for all but the level of noise are found to increase with decreasing chopper frequency, especially below 20 Hz (white noise).

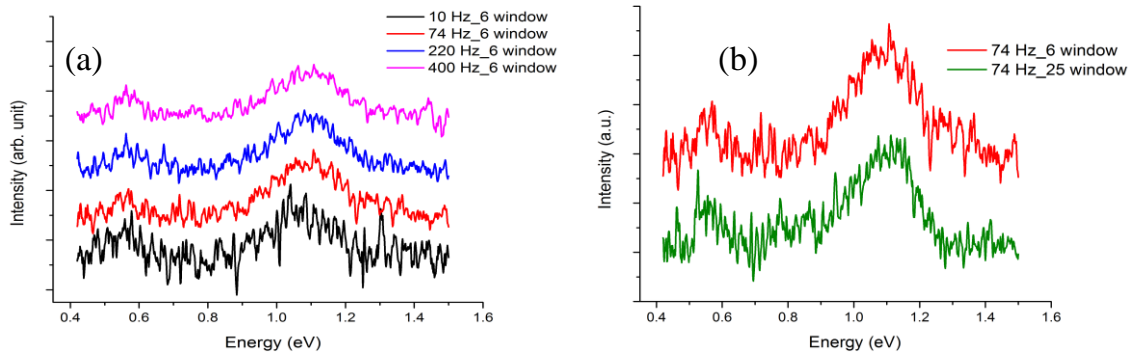


Figure 34. Room temperature μ -PL of ensemble of GaAs-GaAsSb(N) core-shell NWs for (a) different speed of chopper (b) different set of chopper.

4.7.3 Integration time and number of scans

Increasing the number of scans and taking the average instead of increasing the incremental scan time (delay at every point of scan) is found to be more effective in reducing the noise of μ -PL which is shown by the two scans in Fig. 35. This has been done on GaAs-GaAsSb core-shell ensemble of NWs at 4K. Si detector and 10x objective lens were used.

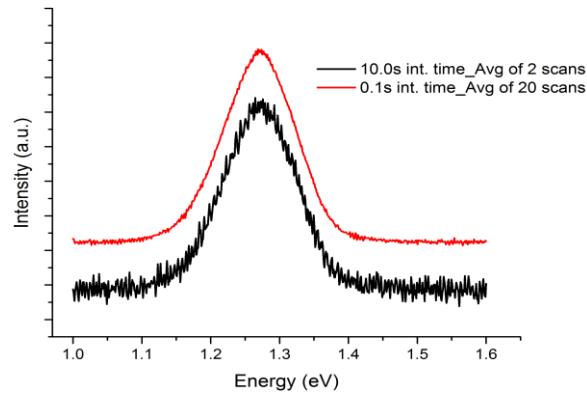


Figure 35. Effect of integration time and average number of scans on μ -PL of NW.

4.7.4 Focusing position

Proper focusing is of extreme importance to get true and good quality μ -PL. Bad focusing may result in extremely low intensity of μ -PL or it may even render false data output. The NWs very often have compositional gradient along their length and sometimes depending on where the actual focus is determines the shape of the μ -PL peaks as well. This is illustrated in Fig. 36. Two dominant peaks are found on GaAs-GaAsSb-GaAs double-shell Sb-12 at.% NWs which appear to change in height as the focusing is done on vertical NWs from top to bottom. The scan was carried out at 4K and Si detector and 10x objective lens were used.

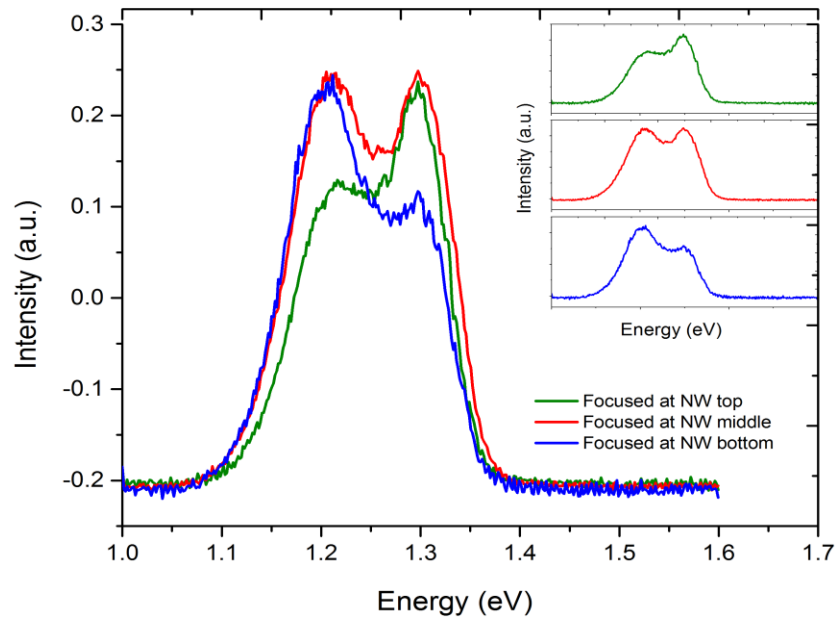


Figure 36. Shape of μ -PL for different focusing position.

4.7.5 Effect of doing SEM before doing μ -PL

Conducting SEM on the NWs before carrying out μ -PL has found to have detrimental effect on the optical properties of the NWs. The degradation in μ -PL is attributed to defects induced by electron bombardment which causes low energy irradiation damage in the material. [47] Usually once SEM is done with excitation voltage of > 0.8 kV, the NWs give either very

poor μ -PL peak or no peak at all (which is found to be most common), both at room temperature and low temperature. Therefore SEM normally is not carried out on the NWs that μ -PL has to be done on and the data is not shown here.

4.8 Special Phenomena and Challenges

This section explains two critical problems that have been frequently encountered. They are- the NW burning phenomena while focusing laser, and the laser peak that sometimes shows up in μ -PL. The former causes to lower the signal intensity in orders of magnitude, while the latter gives a spurious PL signal.

4.8.1 NW melting phenomena

4.8.1.1 Burning of ensemble of NWs

Figure 37 shows the SEM images of ensemble of NWs melting on the bulk substrate in various degree.

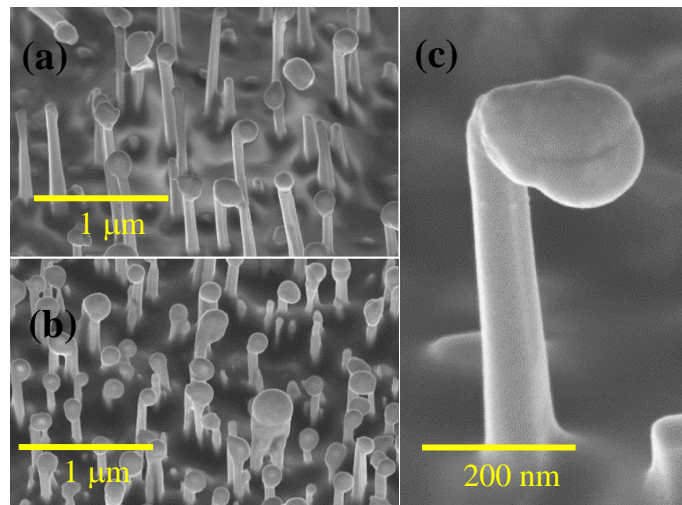


Figure 37. SEM images of ensemble of melted/burnt NWs (a) beginning of melting, (b) partially melted NWs; and (c) a single NW melting from the top.

From the look at Fig. 37 it can be seen that the NWs are rather melted like a candle than actually burnt but we still keep using the term ‘burning’. It has been verified by EDS analysis

that the substrate at the bottom of these burnt NWs have the same composition as that of NWs revealing the fact that they really are getting melted and spreading over the surface and there is no change in NW composition. Further it has been also found that the core-shell and the double shell NWs still retain their characteristic peak on μ -PL, although with much lower intensity. This means that the remaining portion of the NWs are still capable of emission. The NWs are found to burn/melt at much faster rate at 4K under vacuum than at room temperature.

As the laser is focused on the NWs, when the NWs start melting, the signal intensity is decreased in each scan which is depicted in Fig. 38.

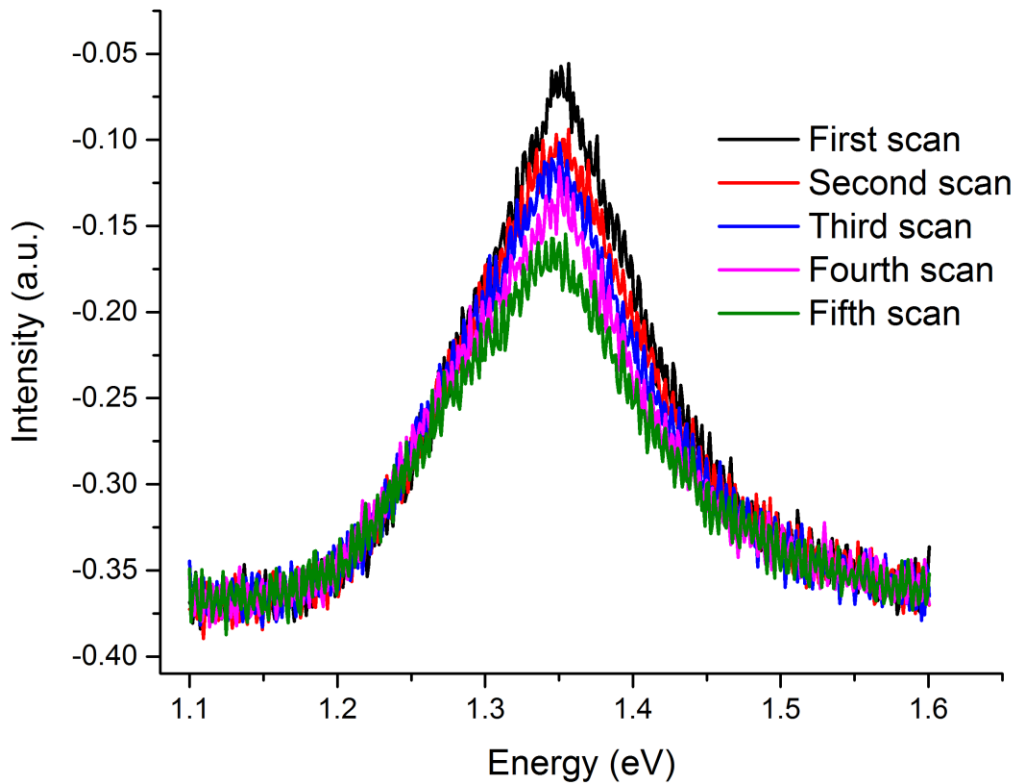


Figure 38. A series of stacked μ -PL scans of ensemble of GaAs-GaAsSb core-shell NWs with Sb-3 at.% composition. Si detector and 50x non-IR lens was used.

The burning phenomena can be suppressed in two ways- either by decreasing the laser intensity, or by increasing the scan speed. Decreasing of the laser intensity can be done either by

changing the lens to the one with lower magnification so that the spot size gets bigger, or by placing a neutral density filter on the path of the laser. Increasing the scan speed can also be done in two ways- either by changing the incremental step delay time, or by increasing the point scan interval energy values. However, both have their own pros and cons. For example, decreasing laser intensity sometimes renders lower emission from the material, very often low enough to make it almost undetectable. On the other hand, there is a limit we can reach in terms of scan speed due to hardware which can still be sufficient to burn the NWs out. And of course, increasing the incremental energy value will give us less detail on μ -PL.

4.8.1.2 Burning of single NWs

Single NWs are found to burn as well, when exposed to the laser for long enough time. But the pattern can be somewhat different than ensemble of NWs. It may either bulge in the corners, form globules, or melt along the edge and spread over the resting surface. When Cu grid is used the conductivity may be sufficient enough to prevent excessive melting. Figure 39 shows the SEM images of some single NWs on Cu grid after μ -PL was done on them.



Figure 39. SEM images showing different modes of NWs burning after being exposed to high intensity laser for μ -PL (a) burning; (b) welding to the resting surface; and (c) spreading melt along edges.

Similar to ensemble of NWs, when the laser is focused on a single NWs for μ -PL, the signal intensity is decreased in each scan which is depicted in Fig. 40.

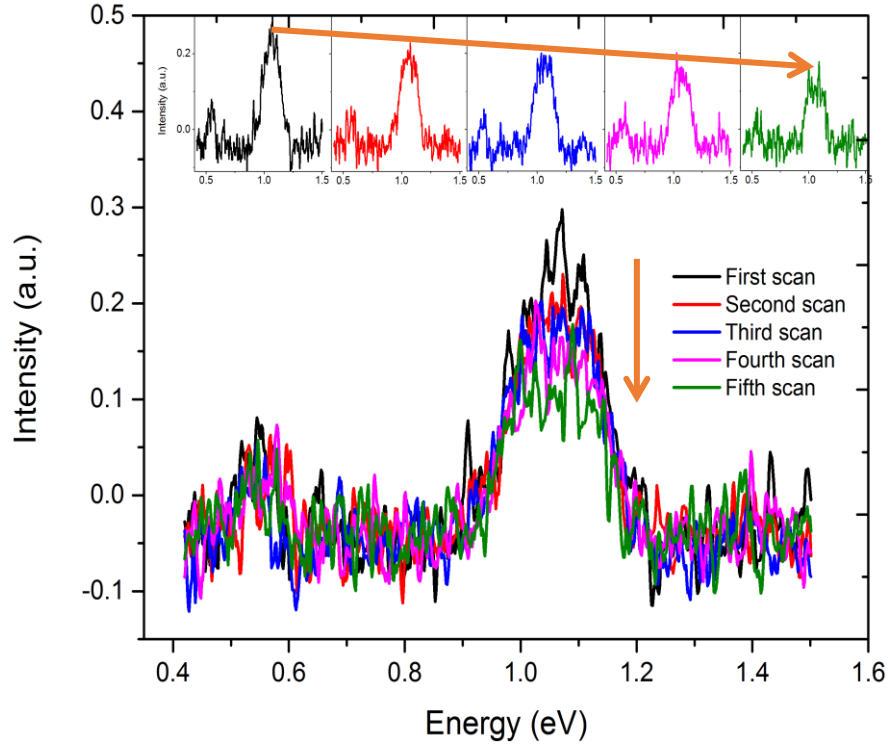


Figure 40. A series of stacked μ -PL scans of a single GaAs-GaAsSb-GaAs double-shell NW at 4K. InGaAs detector and 50x-IR lens was used.

4.8.2 Laser peak

Another phenomena that is frequently encountered while doing μ -PL, especially at 4K, is the appearance of laser peaks on the spectrum. This comes from the grating system of the monochromator.

Figure 41 (a) shows 4K μ -PL of ensemble of GaAs-GaAsSb(N) core-shell NWs at two different positions. One is associated with the prominent laser peaks at 0.674 eV and 1.348 eV where these two peaks are found to be totally absent in the second one. Similar results found for the two NWs in Fig. 41 (b).

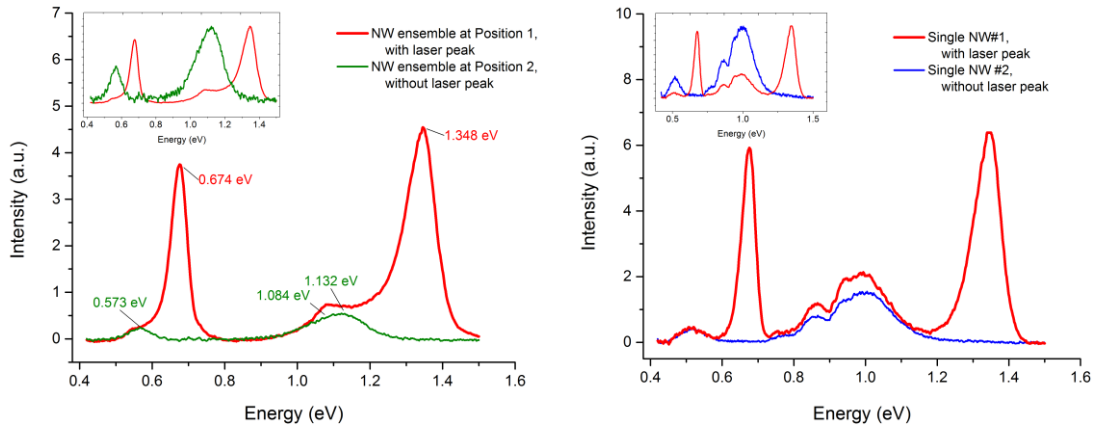


Figure 41. 4K μ -PL of (a) Ensemble of GaAs-GaAsSb(N) core-shell NWs at two different positions. Inset shows the normalized plot of the two spectra. (b) Two different single GaAs-GaAsSb core-shell NWs. Inset shows the normalized plot of the two spectra. InGaAs detector and 50x-IR lens is used for both.

Some useful findings about laser peaks are that they show very small/negligible blue/red shifts with changing laser power intensity (Fig. 42), unlike the NW peaks their intensity do not change over time due to burning (Fig. 43) and they rapidly quenches over 100K (Fig. 44).

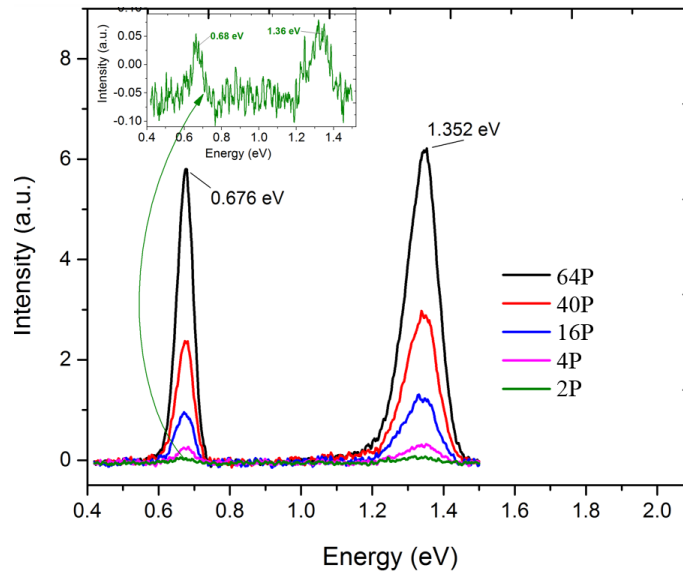


Figure 42. Intensity dependent 4K μ -PL of ensemble of GaAs-GaAsSb core-shell NWs with dominant laser peaks. Inset shows the normalized plot of the spectra at lowest laser intensity.

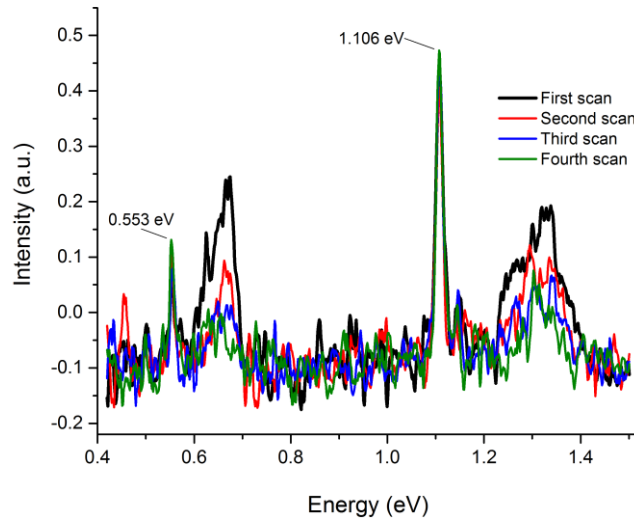


Figure 43. Stacked scans of 4K μ -PL of a single GaAs-GaAsSb core-shell Sb-3.6 at.% composition NW with predominant laser peaks.

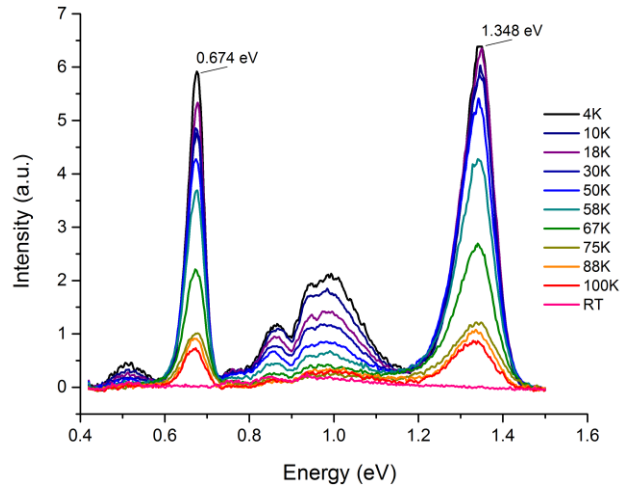


Figure 44. Temperature dependent μ -PL of ensemble of GaAs-GaAsSb core-shell Sb-26.5 at.% NWs with predominant laser peaks.

In this chapter detailed work on μ -PL that have been carried out on different types of GaAsSb(N) samples under different experimental set up and conditions, namely composition and structure of the material, sample type, laser power intensity, temperature, detector type, objective lens, scan speed, number of scans, chopper frequency, and lock-in amplifier sensitivity had been presented. The results are summarized in the next chapter.

CHAPTER 5

Summary and Future Research

In this thesis, room temperature and low temperature (4K) micro-photoluminescence (μ -PL) spectra of GaAs/GaAsSb ensemble NWs of single core-shell and double-shell configurations grown by molecular beam epitaxy are presented. SEM images were taken and the NWs are observed to be curved with increasing Sb composition, which is attributed to the increased strain.

Effect of Sb composition on the μ -PL spectra was carefully studied. Several multi-peaks were fitted for each spectra and the dominant 4K PL peak varied from 1.35 eV to 0.99 eV with Sb concentration varying from 3 at.% to 26 at.%. A band gap alignment in these structures was proposed with the help of intensity dependence of μ -PL spectra at 4K. Shifts in μ -PL spectra verified Type-II transition. With increase in Sb composition type II hetero-alignment transitioned to type I alignment. The peaks in the μ -PL spectra were attributed to two defect levels in the material. Temperature dependent μ -PL spectra were plotted using the Varshni fit which are consistent with the previous data and less temperature dependency of the PL peak energy, desirable feature for optoelectronic device applications.

Experimental setup variables, namely detector type, objective lens magnification, chopper frequency and others on μ -PL of these NWs were also carefully examined to arrive at the optimized set up. InGaAs detector showed superiority over Si detector in all cases. The IR-50x lens was found to render the best μ -PL spectra. Chopper frequency did not show any effect on the overall μ -PL intensity but ~50Hz was found to be optimum for noise reduction. Double-shell NWs showed much higher μ -PL intensity that showed its promise for using at room temperature device applications. Focusing position of the laser on the ensemble of NWs changed the shape of the μ -PL spectra but the peak positions did not change. PL system was suitably

modified to acquire μ -PL spectra from ensemble of NWs to a single NW. The system was made user friendly by adding a suitable attachment exterior to the optical system that facilitated motion of the laser in the nm range. μ -PL spectra of single NW replicated very well the respective NW ensemble, indicative of good compositional homogeneity of the NWs constituting the ensemble. The NWs were found to melt when exposed to high intensity laser for long time that affected the intensity of the μ -PL spectra in each successive scans.

Most of the variables of PL setup were optimized for acquiring μ -PL on both ensemble of NWs and single NW. However, the effect of polarized excitation source has not been examined. This can be done using a polarizer filter on the laser beam. The best laser power intensity has yet to be determined to prevent NW melting upon exposure to laser for long time. The single NW sample preparation technique was developed but not standardized, therefore initiative can be taken to find the optimum time and temperature for ultra-sonication to get single NWs. Outside the boundary of μ -PL, the single NWs can be used to fabricate real life device and electrical measurements can be carried out to find the carrier concentration and other important optoelectronic properties. The initial μ -PL results on nitride samples showed enormous potential of this material for using in high temperature photodetector applications. Further research on this material is highly suggested for near infrared optoelectronic device applications.

References

- [1] "The International Technology Roadmap for Semiconductors," ITRS, 2007.
- [2] P. Yang, R. Yan and M. Fardy, "Semiconductor Nanowire: What's Next?," *Nano Lett.*, vol. 10, no. 5, p. 1529–1536, 2010.
- [3] P. K. Kasanaboina, S. K. Ojha, S. U. Sami, L. Reynolds, Y. Liu and S. Iyer, "Tailoring of GaAs/GaAsSb core-shell structured nanowires for IR photodetector applications," in *Proc. SPIE 9373, Quantum Dots and Nanostructures: Synthesis, Characterization, and Modeling XII*, 937307, San Francisco, California, United States, 2015.
- [4] D. Dheeraj, H. Zhou, A. Moses, T. Hoang, A. v. Helvoort, B. Fimland and H. Weman, "Heterostructured III-V Nanowires with Mixed Crystal Phases Grown by Au-assisted Molecular Beam Epitaxy," in *Nanowires*, Paola Prete (Ed.) ISBN 978-953-7619-79-4, 2010.
- [5] S. G. Ghalamestani, A. M. Munshi, D. L. Dheeraj, B.-O. Fimland, H. Weman and K. A. Dick, "Self-catalyzed MBE grown GaAs/GaAs_xSb_{1-x} core-shell nanowires in ZB and WZ crystal structures," *Nanotechnology*, vol. 24, no. 40, 2013.
- [6] H. Joyce, P. Parkinson, N. Jiang, C. Docherty, Q. Gao, H. Tan, C. Jagadish, L. Herz and M. Johnston, "Electron mobilities approaching bulk limits in "surface-free" GaAs nanowires.," *Nano Lett.*, vol. 14, no. 10, pp. 5989-94, 2014.
- [7] S. Funk, M. Royo, I. Zardo, D. Rudolph, S. Morkötter, B. Mayer, J. Becker, A. Bechtold, S. Matich, M. Döblinger, M. Bichler, G. Koblmüller, J. Finley, A. Bertoni, G. Goldoni and A. G., "High mobility one- and two-dimensional electron systems in nanowire-based quantum heterostructures.," *Nano Lett.*, vol. 13, no. 12, pp. 6189-96, 2013.
- [8] X. Dai, S. Zhang, Z. Wang, G. Adamo, H. Liu, Y. Huang, C. Couteau and C. Soci,

- "GaAs/AlGaAs Nanowire Photodetector," *Nano Lett.*, vol. 14, no. 5, p. 2688–2693, 2014.
- [9] N. Horiuchi, "Nanowire arrays," *Nature Photonics*, vol. 7, no. 166, p. doi:10.1038/nphoton.2013.53, 2013.
- [10] C. Soci, A. Zhang, X. Bao, H. Kim, Y. Lo and W. D., "Nanowire photodetectors," *J Nanosci Nanotechnol*, vol. 10, pp. 1430-49, 2010.
- [11] H. Wang, "High gain single GaAs nanowire photodetector," *Appl. Phys. Lett.*, vol. 103, no. 093101, 2013.
- [12] J. Goldberger, A. I. Hochbaum, R. Fan and P. Yang, "Silicon Vertically Integrated Nanowire Field Effect Transistors," *Nano Lett.*, vol. 6, no. 5, p. 973–977, 2006.
- [13] M. Xin, C. Kelson, Z. Chen, M. Parsian K., W. J. Dennis and L. and Xiuling, "High-Speed Planar GaAs Nanowire Arrays with $f_{\text{max}} > 75$ GHz by Wafer-Scale Bottom-up Growth," *Nano Lett.*, no. DOI: 10.1021/nl503596j, 2014.
- [14] K. Tomioka, M. Yoshimura and T. Fukui, "A III–V nanowire channel on silicon for high-performance vertical transistors," *Nature*, vol. 488, p. 189–192, 2012.
- [15] M. Gudiksen, L. Lauhon, J. Wang, D. Smith and C. Lieber, "Growth of nanowire superlattice structures for nanoscale photonics and electronics," *Nature*, vol. 415, no. 6872, pp. 617-20, 2002.
- [16] J. Bao, M. A. Zimmler and F. Capasso, "Broadband ZnO Single-Nanowire Light-Emitting Diode," *Nano Lett.*, vol. 6, no. 8, p. 1719–1722, 2006.
- [17] S. Thunich, L. Pecht, D. Spirkoska, G. Abstreiter, A. F. i. Morral and A. W. Holleitner, "Photocurrent and photoconductance properties of a GaAs nanowire," *Appl. Phys. Lett.*, vol. 95, 2009.

- [18] A. F. Moses, T. B. Hoang, D. L. Dheeraj, H. L. Zhou and A. T. J. v. Helvoort, "Micro-photoluminescence study of single GaAsSb/GaAs radial and axial heterostructured core-shell nanowires," in *Symposium K, E-MRS 2009 Spring Meeting*, 2009).
- [19] F. Jabeen, V. Grillo, F. Martelli and S. Rubini, "InGaAs/GaAs Core-Shell Nanowires Grown by Molecular Beam Epitaxy," *IEEE JOURNAL OF SELECTED TOPICS IN QUANTUM ELECTRONICS*, vol. 17, no. 4, 2011.
- [20] D. Neamen, *An Introduction to Semiconductor Devices*, McGraw-Hill , 2005.
- [21] B. Streetman and S. Banerjee, *Solid State Electronic Devices* (6th Edition), Prentice Hall, 2005.
- [22] E. H. Nicollian and J. R. Brews, *MOS (Metal Oxide Semiconductor) Physics and Technology*, Wiley-Interscience , 2002.
- [23] P. H. Holloway and G. E. McGuire, *Handbook of Compound Semiconductors*, Noyes Publications, 1995.
- [24] S. M. Sze and M.-K. Lee, *Semiconductor Devices: Physics and Technology*, Wiley, 2012.
- [25] S. W. Koch, M. Kira, G. Khitrova and H. M. Gibbs, "Semiconductor excitons in new light," *Nature Materials* , vol. 5, pp. 523 - 531, 2006.
- [26] C. Kittel, *Introduction to Solid State Physics*, Wiley, 2004.
- [27] M. A. Gilleo, P. T. Bailey and D. E. Hill, "Free-Carrier and Exciton Recombination Radiation in GaAs," *Phys. Rev. B*, vol. 3, no. 3581 , 1971.
- [28] G. P. Agrawal and N. K. Dutta, *Recombination Mechanisms in Semiconductors*, Springer, 1993.
- [29] G. Gilliland, "Photoluminescence spectroscopy of crystalline semiconductors," *Elsevier*

- Materials Science and Engineering: R: Reports*, vol. 18, no. 3-6, p. 99–399, 1997.
- [30] R. G. Hobbs, N. Petkov and J. D. Holmes, "Semiconductor Nanowire Fabrication by Bottom-Up and Top-Down Paradigms," *Chem. Mater.*, vol. 24, no. 11, p. 1975–1991, 2012.
- [31] S. Fortuna, J. Wen and X. Li, "MOCVD Grown III–V Nanowires: In-Plane, self-aligned and transfer-printable," in *IEEE Lasers and Electro-Optics Society, 2008.*, Acapulco, 2008.
- [32] S. Breuer, *Molecular Beam Epitaxy of GaAs Nanowires and their Suitability for Optoelectronic Applications*, Berlin: Ph.D. dissertation, 2011.
- [33] J. Todorovic, H. Kauko, L. Ahtapodov, A. F. Moses, P. Olk, D. L. Dheeraj, B. O. Fimland, H. Weman and A. T. J. v. Helvoort, "The effects of Sb concentration variation on the optical properties of GaAsSb/GaAs heterostructured nanowires," *Semicond. Sci. Technol.*, vol. 28, 2013.
- [34] S. Iyer, L. Reynolds, T. Rawdanowicz, S. K. Ojha, P. K. Kasanaboina and A. Bowen, "A Study of Ga-Assisted Growth of GaAs/GaAsSb Axial Nanowires by Molecular Beam Epitaxy," in *Nanoscience and Nanoengineering: Advances and Applications*, CBC Press, 2014, pp. 31-50.
- [35] M. Jo, M. Sato, S. Miyamura, H. Sasakura, H. Kumano and I. Suemune, "Origin of the blueshift of photoluminescence in a type-II heterostructure," *Nanoscale Research Letters*, vol. 7, no. 654, 2012.
- [36] J. Todorovic, A. F. Moses, D. L. Dheeraj, P. Olk, B. O. Fimland, H. Weman and A. T. J. V. Helvoort, "Correlated micro-photoluminescence and electron microscopy study of a heterostructured semiconductor nanowire," in *Journal of Physics: Conference Series 326*, 2011.

- [37] L. V. Titova, T. B. Hoang, H. E. Jackson, L. M. Smith, J. M. Yarrison-Rice, Y. Kim, H. J. Joyce, H. H. Tan and C. Jagadish, "Temperature dependence of photoluminescence from single core-shell GaAs–AlGaAs nanowires," *Applied Physics Letters*, vol. 89, no. 173126, 2006.
- [38] Y. Varshni, "Temperature dependence of the energy gap in semiconductors," *Physica*, vol. 34, no. 1, p. 149–154, 1967.
- [39] T. B. Hoang, A. F. Moses, H. L. Zhou, D. L. Dheeraj, B. O. Fimland and H. Weman, "Observation of free exciton photoluminescence emission from single wurtzite GaAs nanowires," *Applied Physics Letters*, vol. 94, no. 133105, 2009.
- [40] S. Prucnal, K. Gao, W. Anwand, M. Helm, W. Skorupa and S. Zhou, "Temperature stable 1.3 μm emission from GaAs," *Optics Express*, vol. 20, no. 23, pp. 26075-26081, 2012.
- [41] M. Tajima, T. Iino and K. Ishida, "Above Band-Gap Excitation Process of the 0.6 eV Luminescence Band in GaAs," *Jpn. J. Appl. Phys.*, Vols. 26-2, no. 6, 1987 .
- [42] J. S. Hwang, J. T. Tsai, I. C. Su, H. C. Lin, Y. T. Lu, P. C. Chiu and J. I. Chyi, "GaAsSb bandgap, surface fermi level, and surface state density studied by photoreflectance modulation spectroscopy," *Appl. Phys. Lett.*, vol. 100, no. 222104 , 2012.
- [43] J. M. Dabrowski and M. Scheffler, "Isolated arsenic-antisite defect in GaAs and the properties of EL2," *Physical review. B, Condensed Matter*, vol. 40, no. 15, pp. 10391-10401, 1989.
- [44] J. Bourgoin and T. Neffati, "The energy level of the EL2 defect in GaAs," *Solid-State Electronics*, vol. 43, no. 1, pp. 153-158, 1999.
- [45] M. B. Panish and H. C. Casey Jr., "Temperature Dependence of the Energy Gap in GaAs

- and GaP," *J. Appl. Phys.* , vol. 40, no. 1, p. 163, 1969.
- [46] B. E. A. Saleh and M. C. Teich, *Fundamentals of Photonics*, John Wiley & Sons, Inc., 1991.
- [47] S. Suzuki, "Low-Energy Irradiation Damage," in *Electronic Properties of Carbon Nanotubes*, Atsugi, Kanagawa, Japan, Intech.
- [49] P. K. Kasanaboina, S. K. Ojha, S. U. Sami, C. L. R. Jr. and Y. Liu, "Bandgap Tuning of GaAs/GaAsSb Core-Shell Nanowires Grown by Molecular Beam Epitaxy," *Nanotechnology*, Submitted.